4 Hydrothermal Redistribution

Shallow igneous intrusions produce thermal perturbations in fluid-rich upper crustal rocks which inevitably generate hydrothermal systems in which thermal energy is dispersed by a combination of convective fluid circulation and heat conduction (Norton and Knight 1977). Permeability is the fundamental rock property which controls convective fluid motion and associated chemical and mineral alteration (Norton and Knapp 1977; Norton 1988).

Stable isotope patterns in and around epizonal magmatic intrusions prove that hydrothermal systems can reach many kilometres beyond the magmatic contact zones, with depths of penetration up to 10 km (Taylor 1977, 1979; Criss and Taylor 1986). Important parts of such systems are often affected by little or no petrographically appreciable mineral alteration. High-temperature fluid circulation at >450°C can leave original igneous textures and mineral assemblages in granitic rocks essentially preserved because the assemblage biotite-plagioclase-K-feldspar-quartz is compatible with a broad range of fluid compositions at temperatures even lower than 450°C (Helgeson et al. 1978). A classical example of dominantly high-temperature fluid circulation is the Skaergaard hydrothermal system in which plagioclase (An_{69} to An_{34}) is stable, and only minor amounts of alteration minerals are formed during the waning stages of hydrothermal activity (Norton and Taylor 1979).

In granitic rocks in general and in tin granite suites in particular, abundant secondary fluid inclusions along sealed microfractures in all rock components (including plagioclase) are a widespread phenomenon which points to recrystallization of igneous minerals in equilibrium with aqueous fluids. The same rocks show, however, also to a variable degree - and often predominantly - features of non-equilibrium conditions, i.e. blastesis of secondary hydrous minerals such as sericite/muscovite, chlorite, prehnite, clinozoisite etc. on intergranular spaces, fractures and in replacement aggregates. The term hydrothermal overprint is employed in the following text also in such cases and for such rocks where mineral alteration is not a major feature, but where the geochemical element distribution pattern points to important postmagmatic-hydrothermal fluid interaction and chemical alteration.

Fluid flow in pluton-host rock environments occurs predominantly through percolation networks on all scales (grain boundaries, micro- and macrofractures). The magnitude of fluid flow is proportional to rock

permeability, which has a tendency to decrease during the process of cooling and concomitant mineral precipitation (eventually hydrothermal mineralization). This is a consequence of the generally positive correlation between temperature and solubility for most minerals. Permeability can be drastically increased during the early history of a magmatic-hydrothermal system by sequential exsolution of a magmatic fluid phase which is of fundamental importance in porphyry-type (sensu lato) ore environments.

A characteristic feature of many mineralized granitic rocks is a fracture pattern centred on, and concentrated in, apical portions and late phases of the intrusion suite and their immediately superjacent wall rocks: mineralized stockworks, sheeted veins and breccias, i.e. high-permeability zones in a much less deformed regional environment. This focussed permeability pattern, and corresponding centri-symmetric alteration pattern, is typical of copper porphyry systems (Haynes and Titley 1980; Heidrick and Titley 1982), molybdenum porphyries (White et al. 1981; Carten et al. 1988), tin porphyries (Sillitoe et al. 1975; Grant et al. 1980), as well as tin granites (Bolduan 1963; Baumann and Tägl 1963; Teh 1981; Lehmann 1985; Pollard and Taylor 1986). Therefore, the reason for the release of mechanical energy in porphyry-style environments must be related to the emplacement and solidification of certain granitic intrusions, i.e. endogeneous factors, which of course act on the background of a more or less important regional tectonic framework (Barosh 1968; Linnen and Williams-Jones 1987). The endogeneous generation of mechanical energy ($p \cdot \Delta V$) is a natural consequence of crystallization and/or decompression of a hydrous magma in a shallow crustal environment according to the overall second boiling reaction

$$H_2O \text{ saturated melt} \rightarrow \text{crystals} + \text{aqueous fluid}$$

discussed already by Niggli (1920) and quantified more recently by Burnham (1979a, 1985). The increase in volume ΔV in the above equation results from the fact that the partial molar volume of water dissolved in a silicate melt is much smaller than the molar volume of pure water at the same pressure and temperature (for example: H_2O in albite melt = 22 cm^3/mol, pure H_2O = 78 cm^3/mol at 1 kbar and 800°C; Burnham and Davis 1971). In addition, decompression during fracture formation results in further $p \cdot \Delta V$ energy through expansion of already exsolved H_2O in the magma and exsolution of additional H_2O from interstitial melt.

For magmas that initially contained more than approximately 2 wt% H_2O, the decompression and mechanical energy released upon complete crystallization are sufficient to produce intense fracturing in marginal parts of an intrusion and its roofrocks at depths shallower than approximately 5 km

(Burnham 1985). The initial minimum water content of granitic melts is petrologically constrained by the occurrence of biotite and/or hornblende as a phenocryst phase, which both have a lower stability limit of 2-3 wt% H_2O (Wyllie et al. 1976; Burnham 1979b).

The magmatic origin of the early hydrothermal fluids in granite-related ore systems of the Cu-Mo-W-Sn spectrum has been documented by a large number of isotope studies. The hydrothermal evolution of such systems seems to be characterized by progressive dilution by meteoric water. In tin-tungsten deposits, such a trend has been shown by Grant et al. (1980), Patterson et al. (1981), Jackson et al. (1982), Pollard and Taylor (1986), Sun and Eadington (1987) and Thorn (1988) through stable isotope work, and by Higgins et al. (1987) and Higgins and Sun (1988) with the help of Sr and Nd isotopes. The high salinity of the early hydrothermal solutions of Sn-W ore systems as well as the high acid potential of these fluids, which are capable of large-scale pervasive alteration by mainly H_3O^+-consuming reactions, are in accordance with their magmatic origin.

The hydrothermal alteration pattern in tin-tungsten ore systems is essentially identical to copper porphyry systems of Cordilleran type (Hemley and Jones 1964; Rose and Burt 1979; Burnham and Ohmoto 1980). The high concentrations of boron and/or fluorine in Sn-W systems result, however, in the additional and specific alteration components of tourmaline and fluorite ± topaz. A typical alteration sequence is given in Fig. 43. The temporal overprinting sequence comprises potassic, sodic, sericitic and argillic stages in locally very variable proportions, and is paralleled by the mineral sequence of fracture-controlled tin mineralization which in its early phases is associated with feldspar while later phases are dominated by muscovite or chlorite.

In spite of both widespread fluid flow in granitic rocks and the hydrothermal mobility of tin at high temperatures, granitic rocks in association with tin mineralization often have a tin distribution pattern of predominantly magmatic origin, as deduced from the correlation systematics in the examples of the previous chapter. This must be a consequence of incomplete equilibration with a fluid phase (controlled by permeability, flow rate, and kinetics), and is also a result of the relatively lower mobility of Sn when compared with Pb, Zn, and Cu (Crerar and Barnes 1976; Bourcier and Barnes 1987; Wood et al. 1987). The overall hydrothermal solubilities of galena, sphalerite and bornite/chalcopyrite at high temperature in granitic environment are much greater than that for cassiterite, which explains the generally unsystematic and erratic element pattern of base metals in granites.

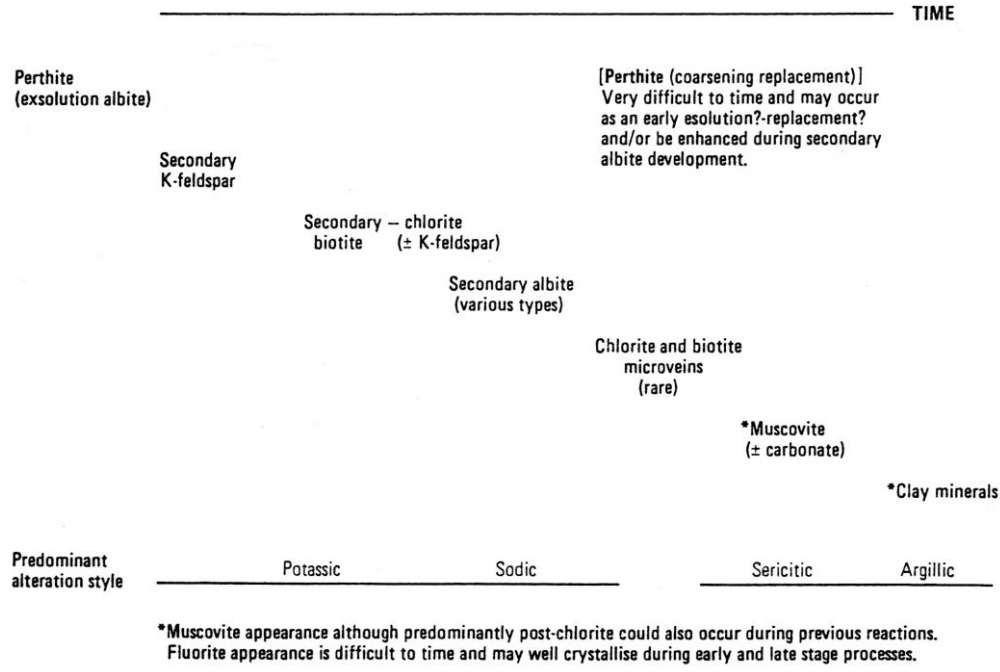

Fig. 43. Timing of main alteration minerals in incipient pervasive alteration of tin granites in the Herberton tin field, Tasmania, Australia. (Pollard and Taylor 1986:1796). This pattern is valid for most tin granites. More advanced degree of alteration results in early formation of tourmaline ± topaz, and blastesis of fluorite over a wide temperature range. Muscovite or zinnwaldite formation begins under early submagmatic conditions

Small-scale metal enrichment in ore deposits and in their hydrothermal haloes must be balanced by zones of large-scale metal depletion. This theoretical condition for ore formation is little documented, and will be addressed in the following examples on tin granites. The most spectacular case of tin depletion is reported for the Tanjungpandan tin granite on Belitung Island (formerly: Billiton), Indonesia. Its anomalously low tin contents were first noted by Cobbing et al. (1986), and subsequent work by Lehmann (1988b) and Lehmann and Harmanto (1990) suggests large-scale hydrothermal tin depletion with an amount of redistributed tin on the order of several million tonnes. The tin depletion zones in the Pilok (Thailand) and Ear Mountain (Alaska, USA) tin fields have much smaller dimensions.

The complementary process of hydrothermal tin enrichment, of which tin ore formation is by definition an integral part, has direct economic impact and is well documented. Our examples are restricted to pervasive tin enrichment patterns and do not include related tin mineralization on major fracture systems. This is, however, an arbitrary distinction which has no point for

greisen deposits, in which the process of pervasive alteration and mineralization is identical. Hydrothermal tin enrichment patterns are presented below for tin mining areas in Thailand (Takua Pa), Malaysia (Kinta Valley), and Bolivia (Chacaltaya and Chorolque).

4.1 Tanjungpandan, Indonesia

The Middle Triassic Tanjungpandan batholith on Belitung Island is associated with major alluvial tin deposits and with minor primary tin mineralization of greisen type (Tikus Mine). Subeconomic quartz-tourmaline-cassiterite veinlets and stockworks are locally abundant. The batholith consists of two petrogenetically different, ilmenite-series rock suites with about the same age of 215 ± 3 Ma (Lehmann and Harmanto 1990): an areally dominating biotite granite suite and a quartz syenite suite of more restricted extent (Fig. 44). The granite suite is composed of three subunits which are, from oldest to youngest: K-feldspar megacrystic medium- to coarse-grained biotite granite (main phase); megacrystic biotite microgranite with medium- to coarse-grained porphyroclasts of plagioclase, K-feldspar, quartz and biotite (first subintrusion); non-megacrystic biotite microgranite (second subintrusion). The quartz syenite suite covers a large compositional spectrum from gabbroic cumulate rocks to hornblende-biotite quartz syenite (main phase) to alkali-feldspar-hornblende granite pegmatite.

The initial $^{87}Sr/^{86}Sr$ ratio of 0.7140 ± 5 for the granite suite together with an $\epsilon_{Nd}(T)$ value of -7.9 suggest intracrustal source material of Proterozoic age (Darbyshire 1988b; Lehmann and Harmanto 1990). Complete equilibration of major element chemistry at a low-pressure minimum-melt composition, i.e. to the shallow emplacement level (Fig. 45), increasingly negative europium anomalies (Fig. 46), and extended magmatic differentiation trends defined by trace elements (Figs. 47 and 48) indicate the important role of crystal fractionation during the magmatic evolution of the biotite granite suite. Chemical data are compiled in Table 3.

The quartz syenite suite is composed of material with a large spread in Sr initials of 0.7049-0.7153 and corresponding initial ϵ_{Nd} values of -5.7 to -6.1 (Lehmann and Harmanto 1990). This suggests a mixing process between mantle and crustal material. Cumulate textures of the gabbro units and trace element variations in the quartz syenite suite point to magmatic fractionation as an important petrogenetic process.

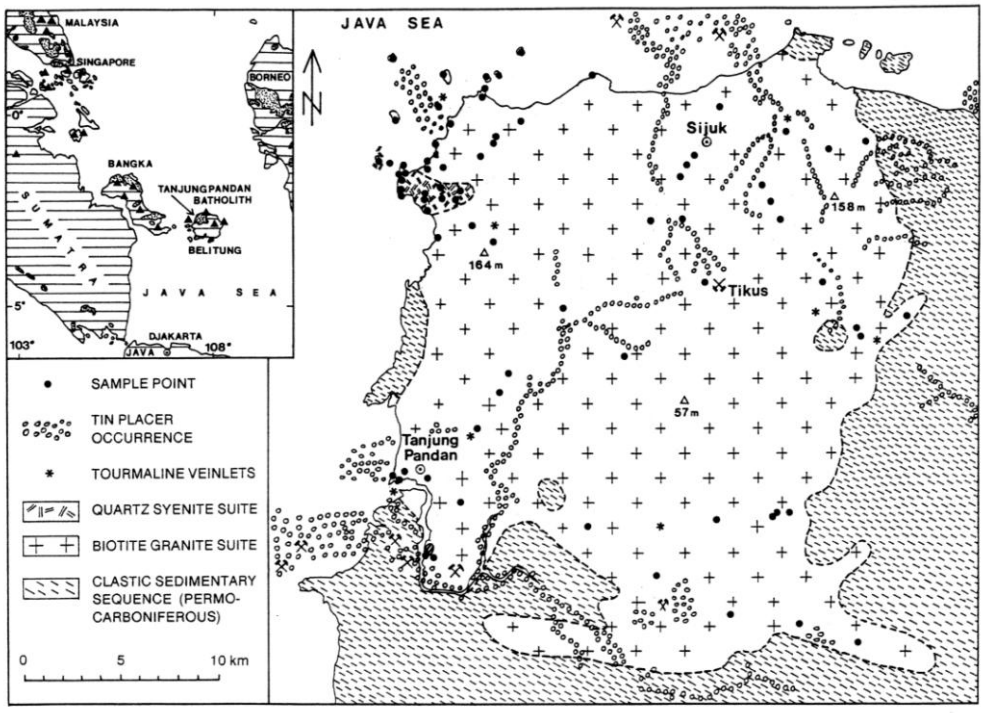

Fig. 44. Location and geology of the Tanjungpandan batholith on Belitung Island, Indonesia. Mine symbols locate past and present tin mining localities. Inset map shows major tin deposits (triangles) in the southernmost part of the SE Asian tin belt, the so-called Tin Islands

The tin content of the biotite granite suite is extremely low, in spite of the high degree of fractionation, the widespread occurrence of quartz-tourmaline-cassiterite veinlets, and the very important alluvial tin concentrations (Fig. 49). The main-phase unit (K-feldspar megacrystic granite) has a mean of 2.8 ppm Sn, the megacrystic microgranite has 4.1 ppm Sn, and the chemically most evolved non-megacrystic microgranite has only 2.1 ppm Sn. The general tin enrichment trend of tin granites, as exemplified by the Erzgebirge granite suite, is included in Fig. 49 for comparison. The average tin contents in the 2-4-ppm range do not satisfy the conventional definition of tin granites which have >15 ppm Sn according to Barsukov (1957).

Contrary to the behaviour of tin, tungsten in the Tanjungpandan rocks is enriched, and gives a scatter distribution with a trend of negative correlation when plotted in terms of the differentiation indicator TiO_2 (Fig. 50), whereas the molybdenum data in Fig. 51 give a trend of decreasing molybdenum content with fractionation. The W and Mo trends are in accordance with the

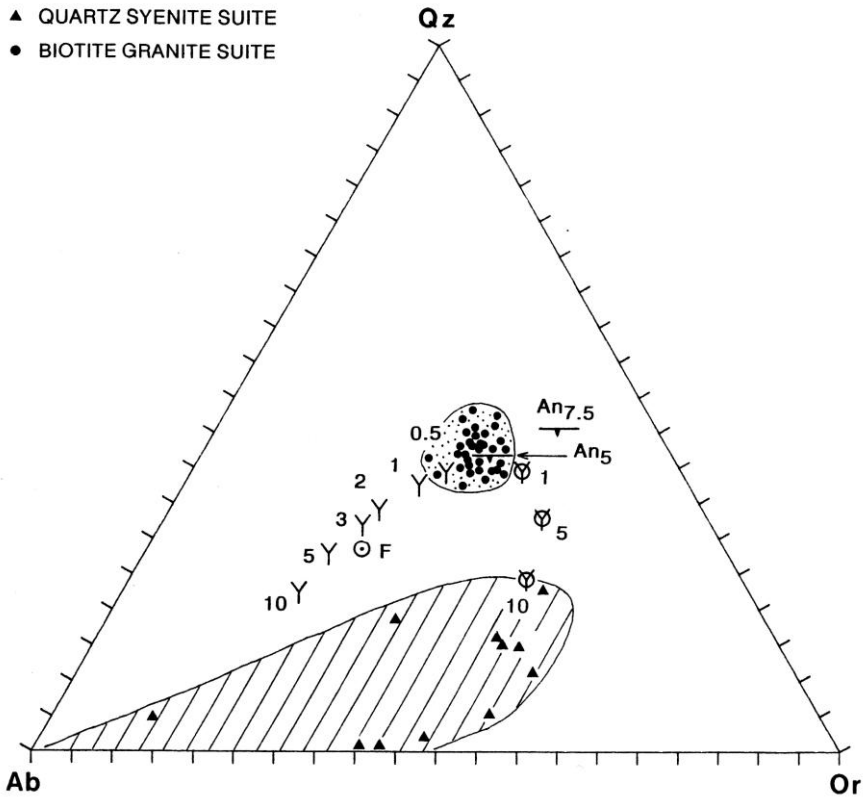

Fig. 45. Normative composition of Tanjungpandan rocks plotted on albite (Ab)-orthoclase (Or)-quartz (Qz) triangle. Y and Φ symbols locate the experimental hydrous and anhydrous granite minima (Qz-Ab-Or-H2O system) at various pressures in kbar (Tuttle and Bowen 1958; Luth et al. 1964; Luth 1969), and two minima points of the Qz-Ab-Or-An-H_2O system at $p_{H2O}=p_{total}=1$ kbar with An_5 and $An_{7.5}$ (James and Hamilton 1969). Point F indicates haplogranitic minimum-melt composition with 1 wt% fluorine and at 1 kbar (Manning 1981)

experimentally predicted magmatic distribution trends in fractionating low-*f*O2 granitic melts, i.e. the dependence of crystal-melt partitioning coefficients of molybdenum and tungsten on oxygen fugacity (Tacker and Candela 1987; Candela and Bouton 1990).

Fig. 46 (next page). REE distribution patterns of the quartz syenite suite and the three subunits of the biotite granite suite, Tanjungpandan batholith, Indonesia

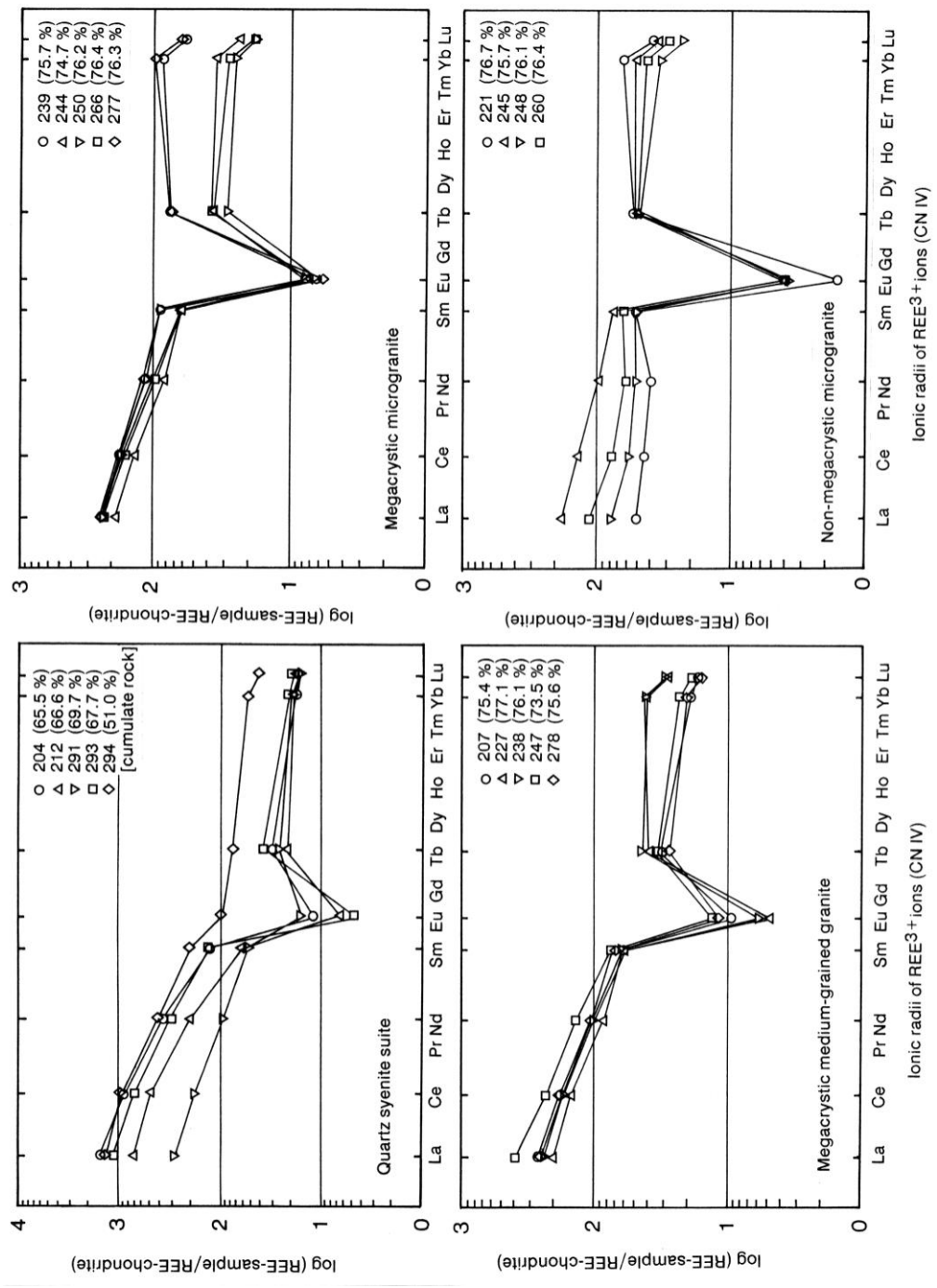

Fig. 46. For legend see previous page

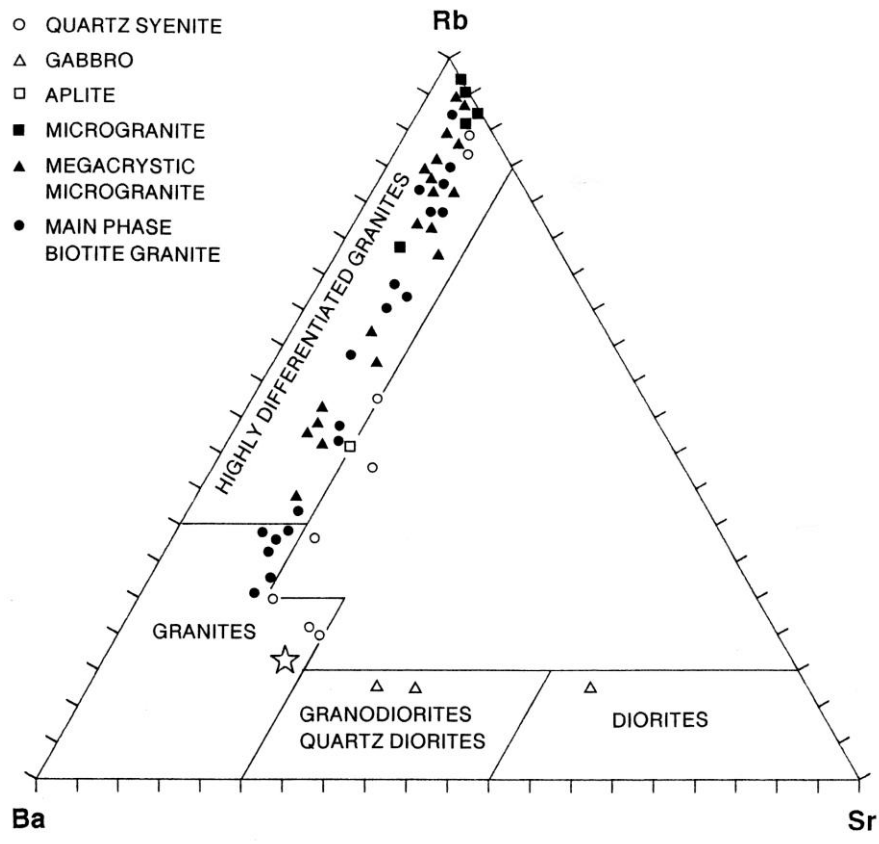

Fig. 47. Rb-Ba-Sr triangle plot of Tanjungpandan rocks. Petrological classification according to El Bouseily and El Sokkary (1975). Star marks world average of granites (Rösler and Lange 1976)

The tin deficiency of the granite compared to the extraordinary wealth of associated tin deposits may be understood in terms of a particularly effective late- or postmagmatic redistribution of tin. The textural evolution of the Tanjungpandan granite suite toward the fine-grained microgranite end-member is a frequent phenomenon in tin granite suites and may be related to a process of quenching by volatile loss (Cobbing et al. 1986; Swanson et al. 1988). Indications of incipient hydrothermal overprint are ubiquitous in the Tanjungpandan batholith; particularly sericitization/muscovitization of feldspars, chloritization of biotite, and poikiloblastic-interstitial blastesis of fluorite and minor tourmaline. Weathering seems to be relatively unimportant, which is also indicated by Fe_2O_3/FeO rock ratios of 0.1-0.01 (Pitfield 1987). These extremely small ratios suggest low $\boldsymbol{f}O_2$ conditions during crystallization or fluid reequilibration of the granite suite, which is also indicated by the abundance of ilmenite (accessory mineral in the rock and of hydrothermal origin on veinlets) and the occurrence of accessory pyrrhotite.

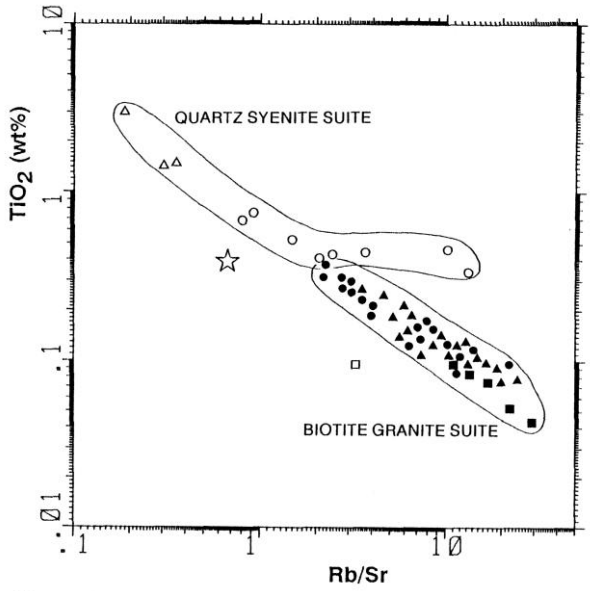

Fig. 48. TiO_2-Rb/Sr variation diagram for Tanjungpandan rock samples. Plot symbols as in Fig. 47

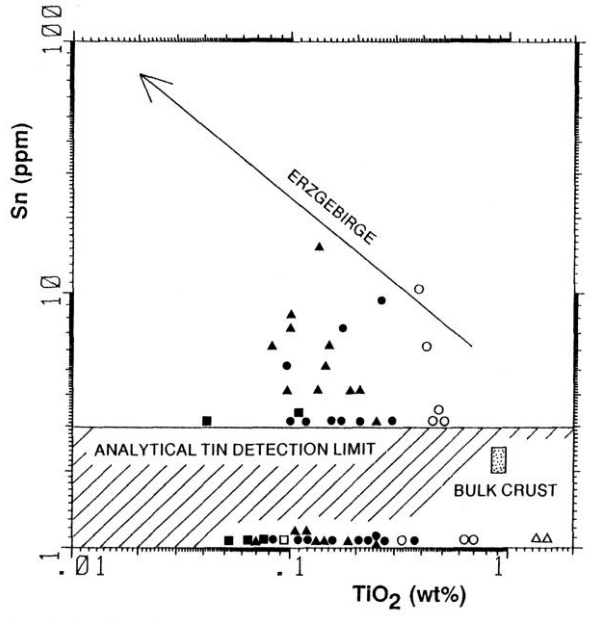

Fig. 49. Tin content in Tanjungpandan rocks as a function of TiO_2 (wt%). General magmatic tin enrichment path in tin granites as exemplified by the Erzgebirge trend. Plot symbols as in Fig. 47. Sample points below the analytical detection limit represent values of <3 ppm Sn.

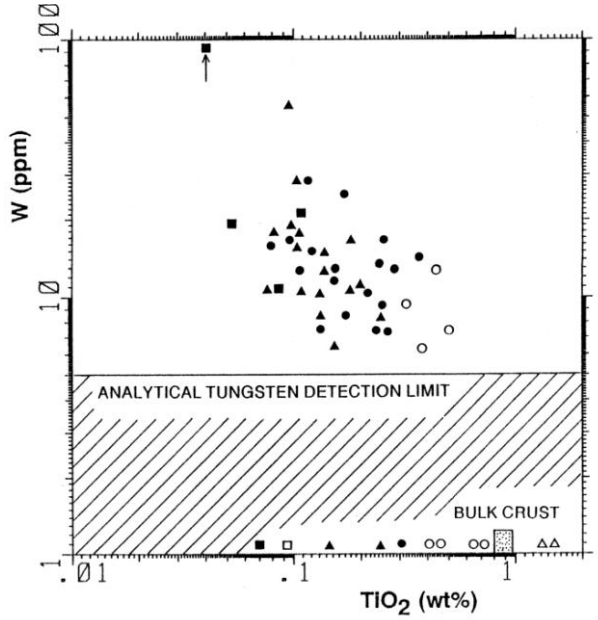

Fig. 50. Variation of tungsten as a function of TiO_2 (wt%) for Tanjungpandan rocks. Sample points below analytical detection limit represent values of <5 ppm W. Plot symbols as in Fig. 47.

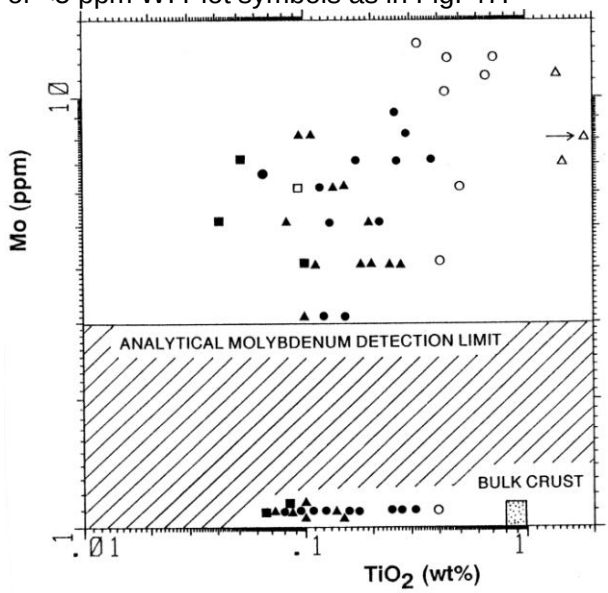

Fig. 51. Variation of molybdenum as a function of TiO_2 (wt%) for Tanjungpandan rocks. Sample points below analytical detection limit represent values of <3 ppm Mo. Plot symbols as in Fig. 47

The dramatic dependence of tin mobility on oxygen fugacity has been discussed in Chapter 2.7 and provides an explanation for the exceptionally large-scale tin depletion in the Tanjungpandan granite suite. The neighbouring tin granites on Bangka and Singkep have similar scatter distributions of tin (Fig. 52). These granites have very low Fe_2O_3/FeO rock ratios of <0.1 as well (Pitfield 1987).

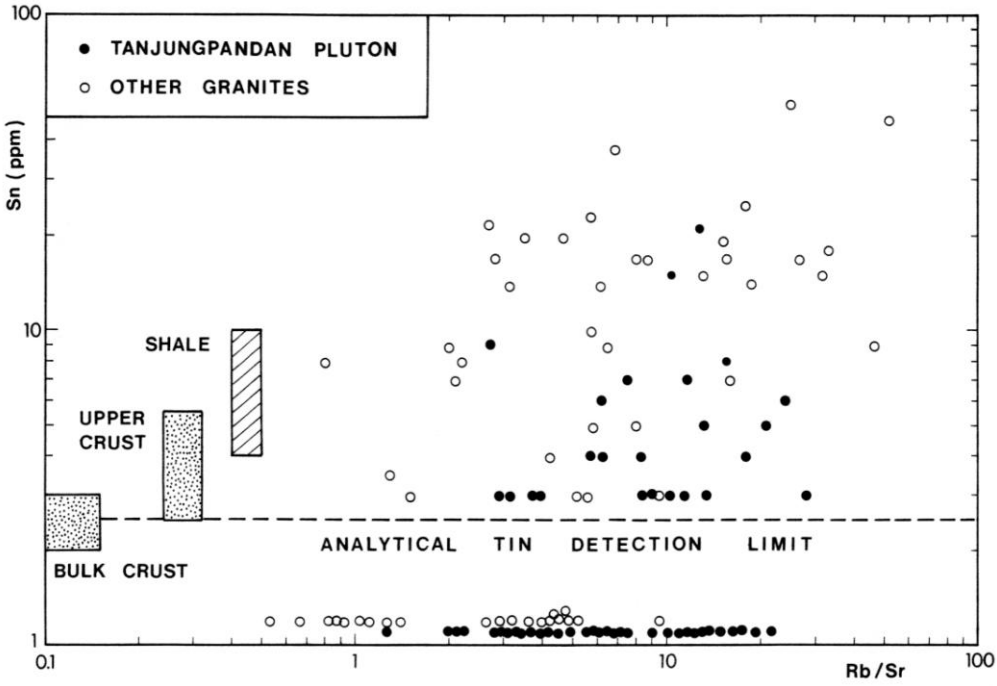

Fig. 52. Tin content as a function of Rb/Sr for Tanjungpandan granitic rocks, Belitung Island, and neighbouring tin granites on Bangka and Singkep Islands. Data from Pitfield (1987)

The primary-magmatic tin content of the Tanjungpandan batholith can be estimated from comparison with the general tin evolution path in less disturbed tin granites (Fig. 49). A conservative estimate arrives at a bulk tin content of around 15 ppm Sn, taking into account the evolved differentiation range of the Tanjungpandan rocks. This figure must be compared with the actual tin content of only 3 ppm. The missing 12 ppm Sn, integrated over the surface exposure of 700 km^2 with an arbitrary depth figure for the hydrothermal depletion system of 500 m, would represent an amount of 10 million tonnes of tin; about ten times the historical tin output of Belitung Island. Of course, only a small part of all redistributed tin is focussed into

Table 3. Chemical composition of major rock groups of Tanjungpandan batholith

	Quartz syenite suite		Biotite granite suite			
	Gabbro (n = 3)	Quartz syenite (n = 8)	Main phase granite (n = 19)	Megacrystic microgranite (n = 19)	Micro-granite (n = 5)	Aplite (n = 1)
Major elements in weight percent (mean ± 1 standard deviation):						
SiO2	48.65 ± 2.04	65.14 ± 3.02	75.54 ± 1.10	76.10 ± 0.78	76.00 ± 0.67	75.84
TiO2	1.85 ± 0.86	0.47 ± 0.13	0.18 ± 0.08	0.14 ± 0.05	0.07 ± 0.03	0.09
Al2O3	14.72 ± 2.52	16.11 ± 0.98	12.20 ± 0.38	12.06 ± 0.44	12.61 ± 0.25	12.63
Fe2O3	10.60 ± 4.31	4.03 ± 1.58	1.79 ± 0.40	1.63 ± 0.29	1.05 ± 0.23	0.71
MnO	0.20 ± 0.06	0.11 ± 0.05	0.04 ± 0.01	0.04 ± 0.01	0.03 ± 0.01	0.02
MgO	6.05 ± 2.80	0.22 ± 0.18	0.13 ± 0.11	0.07 ± 0.08	0.02 ± 0.02	0.04
CaO	11.24 ± 2.72	2.17 ± 0.53	1.29 ± 0.28	1.05 ± 0.15	1.05 ± 0.11	0.75
Na2O	2.56 ± 0.95	3.62 ± 0.71	2.46 ± 0.23	2.51 ± 0.20	3.01 ± 0.32	2.15
K2O	1.68 ± 1.29	6.99 ± 0.87	5.23 ± 0.33	5.20 ± 0.29	5.10 ± 0.53	6.72
P2O5	0.34 ± 0.13	0.07 ± 0.05	0.03 ± 0.02	0.02 ± 0.01	0.01 ± 0.01	0.02
L.O.I.	1.54 ± 0.72	0.55 ± 0.10	0.65 ± 0.10	0.73 ± 0.12	0.67 ± 0.08	0.74
Trace elements in ppm (mean and range):						
Ba	403 (94-748)	314 (6-574)	256 (24-568)	134 (<5-418)	24 (<5-104)	265
Ce	107 (73-163)	322 (93-800)	154 (66-228)	122 (84-165)	61 (33-113)	63
Cs	3	3 (1-6)	7 (3-9)	10 (8-12)	6	-
Cu	95 (12-224)	7 (<5-24)	<5 (<5-27)	<5 (<5)	<5 (<5)	<5
F	707 220-1425	273 (110-575)	1662 830-2550	1856 1215-2630	1762 1405-2140	715
La	83 (66-101)	212 (59-532)	95 (54-142)	77 (54-108)	40 (12-68)	25
Li	31	18 (13-22)	35 (22-46)	51 (38-63)	34 (24-44)	-
Mo	8 (5-11)	9 (<3-13)	4 (<3-9)	4 (<3-8)	4 (<3-7)	6
Nb	15 (9-19)	21 (11-31)	15 (12-22)	17 (10-21)	19 (13-30)	6
Ni	40 (10-80)	<5 (<5)	<5 (<5)	<5 (<5)	<5 (<5)	<5
Pb	7 (<5-18)	32 (25-41)	33 (17-48)	40 (26-55)	52 (37-59)	40
Rb	93 (37-155)	228 (173-313)	355 (255-501)	399 (312-504)	408 (356-447)	318
Sn	<3 (<3)	4 (<3-10)	3 (<3-9)	4 (<3-15)	2 (<3-3)	2
Sr	330 (204-490)	124 (16-228)	72 (24-127)	48 (21-104)	26 (15-39)	102
Th	19 (<5-41)	62 (29-107)	75 (52-89)	77 (52-96)	66 (42-108)	25
U	7 (4-10)	10 (6-12)	13 (4-23)	14 (5-21)	19 (15-26)	2
V	212 (93-363)	12 (1-31)	11 (1-26)	9 (4-21)	6 (1-13)	7
W	<5 (<5)	5 (<5-12)	12 (<5-27)	14 (<5-53)	104 (<5-467)	<5
Y	38 (31-44)	43 (32-67)	85 (41-201)	81 (48-167)	114 (79-181)	16
Zn	82 (47-113)	56 (25-91)	24 (16-36)	20 (15-30)	12 (9-18)	16
Zr	219 (161-320)	653 (365-950)	165 (90-251)	145 (101-226)	81 (24-139)	53
DI	29.3 ± 13.0	83.4 ± 3.9	89.2 ± 2.1	90.5 ± 1.2	91.8 ± 0.6	93.6
ALUM	0.57 ± 0.14	0.92 ± 0.06	1.01 ± 0.02	1.03 ± 0.02	1.02 ± 0.03	1.04

Note: Besides some complementary F, Cs, Li analyses all data by X-ray fluorescence spectrometry. N is number of samples, Fe_2O_3 is total iron, DI is Thornton-Tuttle differentiation index (normative Qz + Ab + Or), ALUM is index of alumina saturation (molecular $Al_2O_3/CaO + Na_2O + K_2O$).

zones amenable to tin mining. Depending on the local parameters of the hydrothermal circulation system, generally a large part of the redistributed tin is fixed in positive geochemical haloes which have not been sampled in the Tanjungpandan case. Unexposed or little exposed tin granite plutons commonly have a cap of greisen alteration in place, of which the tin-tungsten Tikus deposit is the only known relic in the Tanjungpandan batholith (Jones et al. 1977; Schwartz and Surjono 1988). The erosional level of the Tanjungpandan situation seems to be in an optimal balance between very advanced erosion of lode deposits/primary tin enrichments and a long history of alluvial concentration of cassiterite in residual lag gravel deposits (Aleva 1985).

The exposure of the Tanjungpandan batholith (25 x 30 km in size) at a level perhaps well below the top of the "productive" hydrothermal tin enrichment zone would explain the unusual low-tin granite situation as compared to less eroded tin-bearing systems in Malaysia, Thailand, Burma, Cornwall, Bolivia, etc. which are characterized by high-tin tin granites with average tin contents of generally >15 ppm. The exposure level of the Tanjungpandan granite may therefore provide the rare opportunity to look into the deeper parts of a hydrothermal tin system dominated by tin depletion, with at the same time relics of the upper part of such a system (dominated by tin enrichment) preserved by a fortunate geomorphologic situation of multistage alluvial reworking. The abundant subeconomic quartz-tourmaline-cassiterite veinlets are seen as the root zones of the eroded greisen- and lode-mineralized roof zones.

The reverse case of a particularly effective hydrothermal molybdenum mobilization accompanied by invariable tin levels has been documented by Haffty and Noble (1972) for strongly oxidized rhyolitic rocks in Nevada. Although the complementary behaviour of Mo and Sn as a function of oxygen fugacity was not established at that time, the element patterns in Fig. 53 correspond to the expected trends for hydrothermal alteration at high fO_2 (Fe_2O_3/FeO of the rhyolitic rocks 0.8-2.5; Noble et al. 1968).

Hydrothermal depletion of molybdenum has also been demonstrated more recently for the Miocene rhyolitic ash-flow/dome volcano complex which hosts the Pine Grove porphyry molybdenum deposit in Utah (Keith and Shanks 1988). The ash-flow tuffs are relatively oxidized (log fO_2 reconstructed from Ti-Fe-oxide phases: -16.1 ± 0.7 at 670°C) and show a distinct Mo depletion in even weakly devitrified and hydrated ash samples, with Na content taken as a measure of hydrothermal leaching (Fig. 54). The diagram suggests that molybdenum is leached from the tuff samples in a

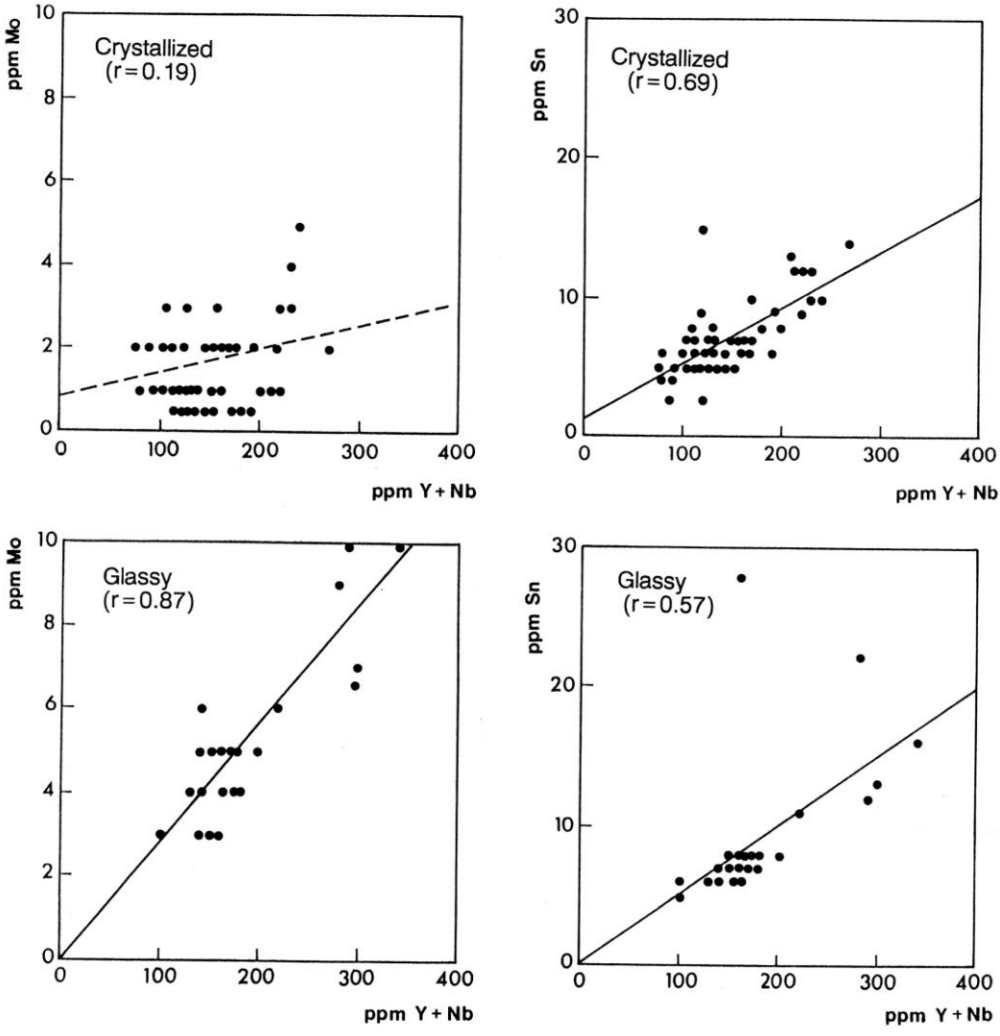

Fig. 53. The different behaviour of tin and molybdenum during devitrification of Tertiary magnetite-series rhyolitic lavas and tuffs in Nevada: constant Sn levels versus hydrothermal Mo depletion. Data from Haffty and Noble (1972). The parameter Y+Nb (ppm) was used by Haffty and Noble (1972) as indicator of fractionation, not affected by hydrothermal overprint. The correlation of Y+Nb vs. Mo and Sn is 0.87 and 0.57 (n=29), respectively, in rhyolitic glass samples, whereas the same correlation in devitrified (crystallized) samples is 0.19 for molybdenum (no significant correlation, i.e. Mo scatter distribution) and 0.69 for tin (undisturbed magmatic correlation trend) (n=57)

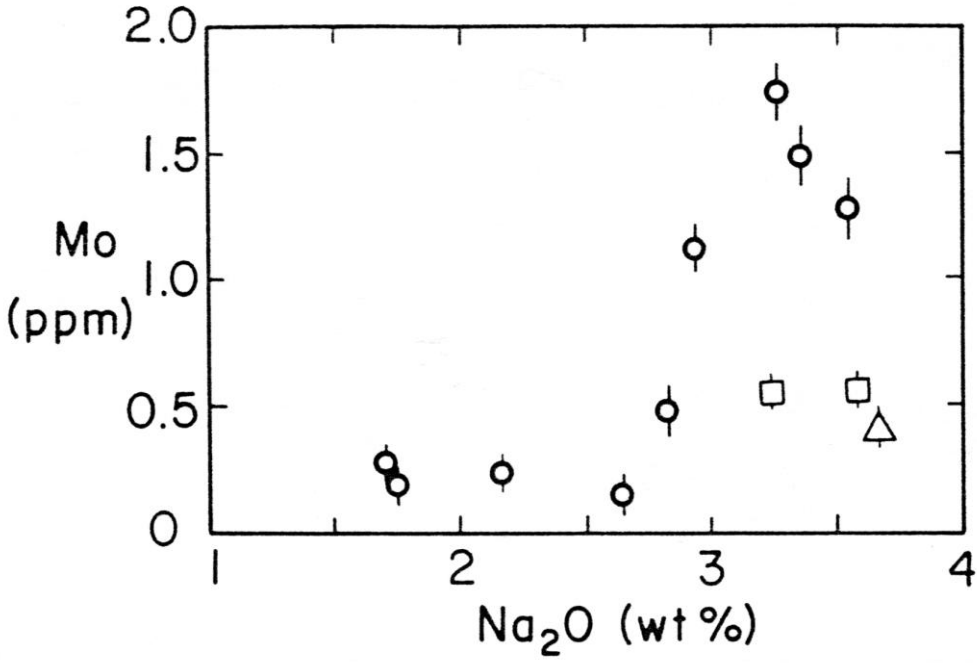

Fig. 54. Whole-rock analyses of molybdenum (ppm) versus Na_2O (wt%) for igneous rocks from the mid-Tertiary Pine Grove volcano-plutonic system in Utah, USA: concomitant leaching of both Na and Mo. Heavy circles represent partly devitrified ash-flow units; the squares and the triangle are rhyolite porphyry samples. Short vertical lines at each data point give analytical uncertainty. (Keith and Shanks 1988:415)

fashion similar to sodium. Samples with magmatic Na concentrations contain about 1.6 ± 0.2 ppm Mo, strongly devitrified samples of the tuff sequence contain only 0.2 ± 0.1 ppm Mo. Fresh porphyry samples contain about 0.5 ± 0.1 ppm Mo, which is thought to be a result of another removal process, i.e. transfer of Mo by an exsolving magmatic fluid phase (Keith and Shanks 1988).

4.2 Pilok, Thailand, and Hermyingyi, Burma

The tin-tungsten mining districts of Pilok in western Thailand and of neighbouring Hermyingyi in Burma (Fig. 31) are centred on highly evolved alkali-feldspar aplogranite stocks of Cretaceous-Tertiary age. The mineralized stocks are exposed in their uppermost portions with surfaces of <1 km^2 and intrude locally foliated K-feldspar megacrystic biotite granite (Border Range main-phase granites) and a Paleozoic sequence of low-grade metamorphic

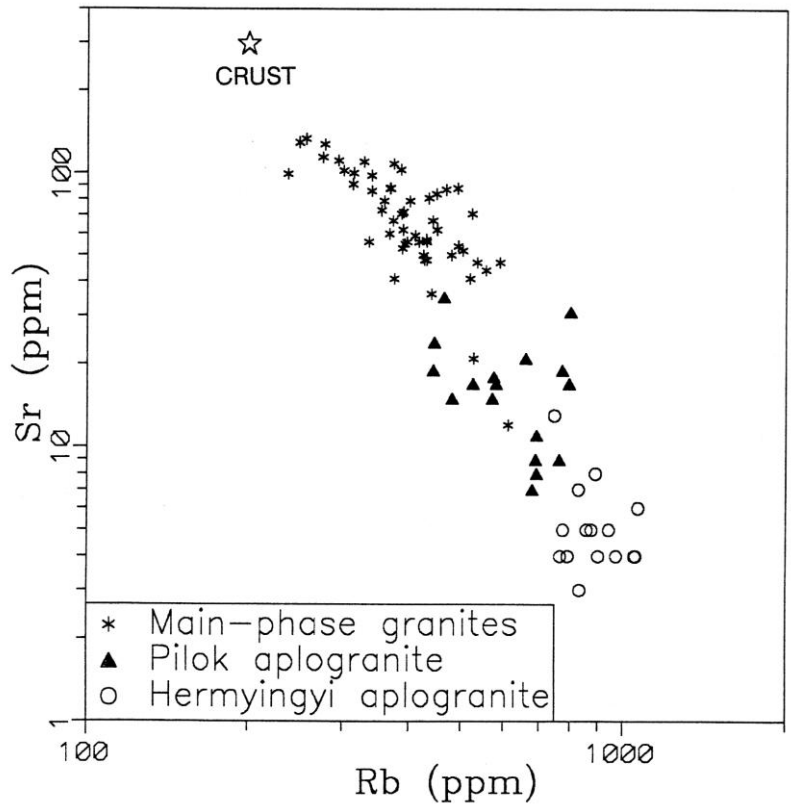

Fig. 55. Rb-Sr variation diagram for granitic rocks from central Thailand and Burma. Open star locates composition of average granitic rocks (Vinogradov 1962, cited in Rösler and Lange 1976). Data from Lehmann (1988a) (Thailand and part of Hermyingyi), and Cobbing et al. (1988) (part of Hermyingyi)

Paleozoic sediments. The alkali-feldspar granite stocks are the product of both advanced fractional crystallization and of fluid overprint in a transitional magmatic-hydrothermal situation; they have the granoblastic (partly symplectic) mineral assemblage quartz-microcline-albite-muscovite-tourmaline-spessartine-fluorite-beryl. The Sr isotope pattern of the Hermyingyi stock is undisturbed and defines a nine-point isochron age of 59 ± 2 Ma and an initial ratio of 0.735 ± 8 (Darbyshire and Swainbank 1988), whereas Sr isotope ratios from the Pilok stock give a scatter distribution and point to exchange with external strontium (Höhndorf unpubl. data). Mineralization consists of disseminations, stockworks, and veins with an ore association composed mainly of arsenopyrite, chalcopyrite, sphalerite, pyrite, cassiterite, and wolframite. Minor components are pyrrhotite, stannite, bismuthinite, bismuth, molybdenite, and scheelite. The gangue assemblage is quartz-

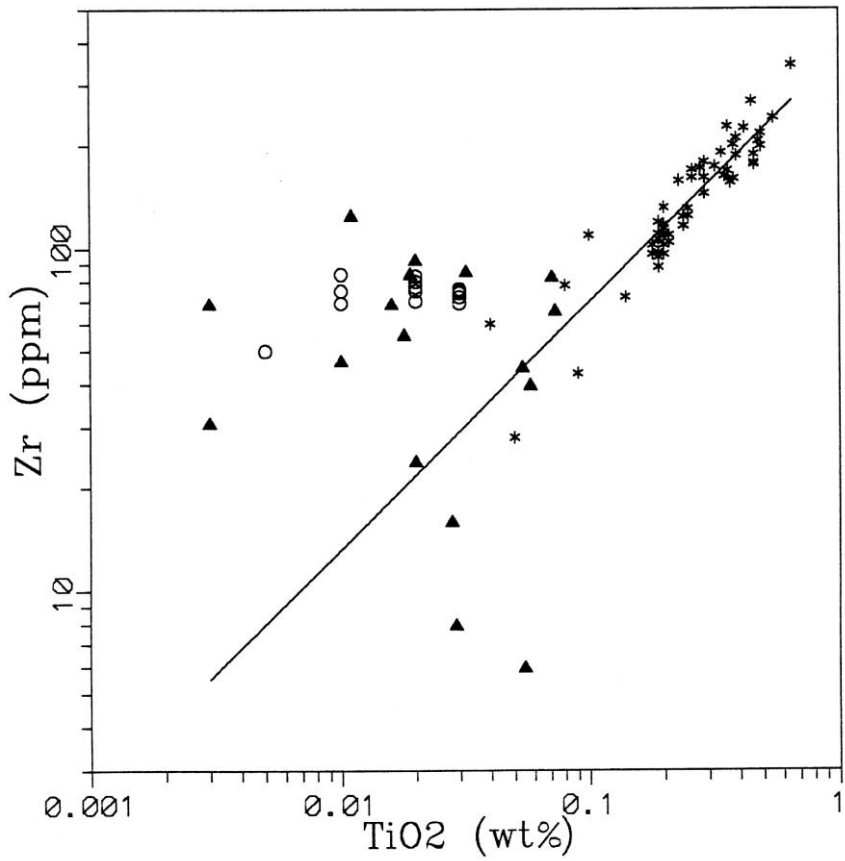

Fig. 56. Zr-TiO_2 variation diagram for granitic rocks from central Thailand and Burma. Symbols as in Fig. 55

muscovite-tourmaline-beryl-fluorite-apatite. Pervasive kaolinization is locally strongly developed.

Chemical data of the Pilok and Hermyingyi aplogranites in comparison with granites from the Border Range (main-phase granites of the western granite province), the Rayong Pluton (Main Range province), and the Loei and Chanthaburi granites (eastern granite province) are compiled in Table 4; the general location of these sample groups is given in Fig. 31. Major and trace element concentrations and distribution patterns of the aplogranites indicate an exceptionally high degree of fractionation. The Rb-Sr diagram of Fig. 55 defines a position of the fluid-modified aplogranite samples in the extension of the magmatically controlled trend of the main-phase granites. The Zr-TiO_2 variation pattern of the aplogranites is a scatter distribution at the lower part of the extrapolated magmatic trend (Fig. 56). The large scatter implies the absence of any significant control by fractional crystallization of zircon, which in granites is usually an inclusion phase in biotite, or of biotite/Ti-Fe-oxides.

Table 4. Arithmetic means of chemical data for granitic rocks of central Thailand and Burma. Data from Lahmann and Mahawat (1989)

	Loei grano-diorites (n = 7)	Chan-thaburi granites (n = 29)	Rayong granite (n = 25)	Border range granites (n = 20)	Pilok aplo-granite (n = 17)	Hermyingyi aplo-granite (n = 6)
Oxides (wt%)						
SiO_2	63.34	70.28	72.60	73.42	76.18	76.00
TiO_2	0.59	0.41	0.31	0.25	0.03	0.03
Al_2O_3	15.86	14.34	13.80	13.53	13.16	12.83
Fe_2O_3	4.99	3.38	2.08	1.88	0.52	0.99
MnO	0.09	0.06	0.05	0.06	0.07	0.23
MgO	2.20	0.46	0.66	0.35	0.01	0.01
CaO	4.62	2.06	1.26	1.00	0.30	0.50
Na_2O	3.43	3.76	2.74	2.92	3.92	3.45
K_2O	2.99	3.96	5.00	5.11	4.43	4.38
P_2O_5	0.17	0.09	0.16	0.09	0.04	0.01
L.O.I.	1.22	0.68	0.83	0.88	0.73	0.98
Trace elements (ppm)						
Ba	538	368	476	255	13	33
Ce	45	79	66	85	5	47
Cr	29	<15	20	<15	<15	<15
Cu	20	15	6	5	30	18
La	<20	39	26	34	11	81
Nb	7	9	15	24	47	36
Ni	15	8	15	8	9	<5
Pb	11	34	49	87	90	81
Rb	99	207	351	442	625	979
Sn	3	7	10	14	27	72
Sr	381	118	81	65	17	4
Th	10	23	24	43	21	37
U	<5	7	8	19	31	24
V	109	24	25	19	<15	<15
Y	22	51	42	63	102	190
Zn	49	68	32	47	69	135
Zr	147	256	146	149	53	75
D.I.	64	82	86	89	95	93

Note: Analyses by X-ray fluorescence spectrometry. Fe_2O_3 is total iron. D.I. is Thornton-Tuttle differentiation index. L.O.I. is loss on ignition.

Positive correlation coeffcients for Zr with Y (r=0.60; number of samples=25), Th (0.73), and Ce (0.55), together with the presence of accessory xenotime and the absence of zircon point to a mineralogical control of the zirconium levels by xenotime. Titanium correlates with Fe (r=0.61), Mg (0.62), Na (-0.65), D.I. (-0.58) and may therefore be used tentatively as an indicator of fractionation.

The tin content of the rock as a function of TiO_2 and Rb/Sr is shown in Fig. 57. The samples from the Rayong and Border Range granites (main-phase granites) display a systematic trend that can be interpreted in terms of progressive magmatic enrichment of tin which is statistically significant at a confidence level of >99.9% with a correlation coefficient r(logTiO_2-logSn) -0.62, and r(logRb/Sr-logSn) 0.65, respectively (50 samples). This is a trend very similar to granite populations from other tin provinces (Lehmann 1982). Three samples of the original sample population (total of 53) are not included in this trend because they have anomalously low tin contents combined with high Rb/Sr and low TiO_2, and plot in the compositional field characterized by fluid interaction. This fluid-controlled field locates all aplogranite samples and is characterized by a scatter distribution in an open system. The tin concentration of these samples is anomalously low relative to their degree of differentiation and is interpreted to be due to removal of tin by fluid interaction. It is further inferred that this mobilized tin is then deposited in fracture systems that are also the main channels for fluid movement.

A geochemical balance of the system can be made when the tin mineralization is taken into account. The original mean content of tin of the Pilok aplogranites can be estimated from the general magmatic correlation trend in Fig. 57. A primary content of 85 ppm Sn in the magma results (standard deviation 35-269 ppm). Compared to the actual mean content of tin, which is 27 ppm (range 0-64 ppm Sn), there is a difference of 58 ppm Sn. This figure provides a basis for estimation of the potential for tin ore of the Pilok

---

Fig. 57 (next page). Tin as a function of TiO_2 and Rb/Sr in granitic rocks from central Thailand and Burma. The main-phase granites (Rayong pluton and Border Range granites) define a tin enrichment trend (solid correlation line) which corresponds to the general magmatic trend for tin granites (Lehmann 1982). Rock compositions in the stippled field (limited by dashed line) are controlled by fluid interaction and are characterized by tin depletion. Note tin deficiency between extrapolated magmatic trend and fluid-modified aplogranite samples. The tin enrichment trends are defined by the correlation lines $\log[Sn] = -0.86\log[TiO_2] + 0.57$, and $\log[Sn] = 0.77\log[Rb/Sr] + 0.49$

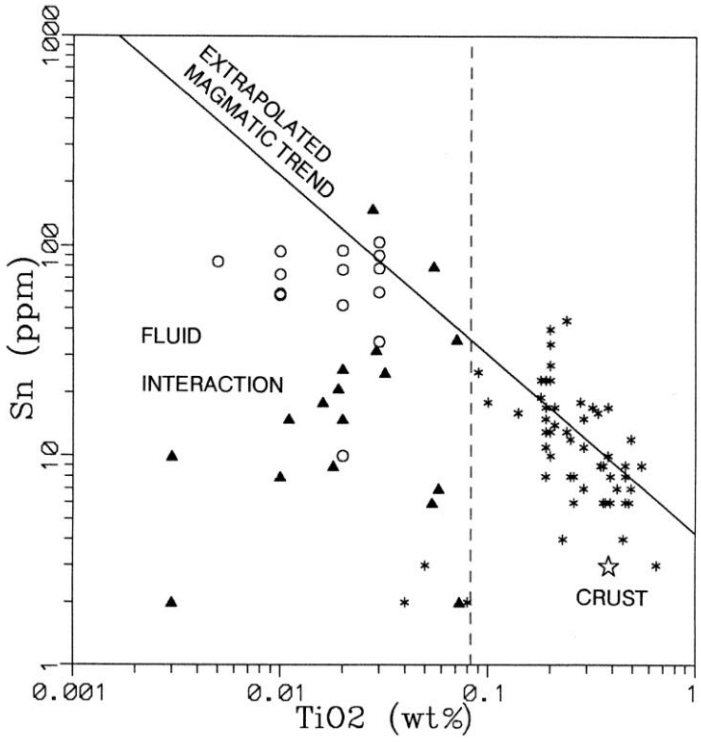
EXTRAPOLATED
MAGMATIC TREND
FLUID
INTERACTION
CRUST
Sn (ppm)
TiO2 (wt%)
1000
100
10
1
0.001
0.01
0.1
1

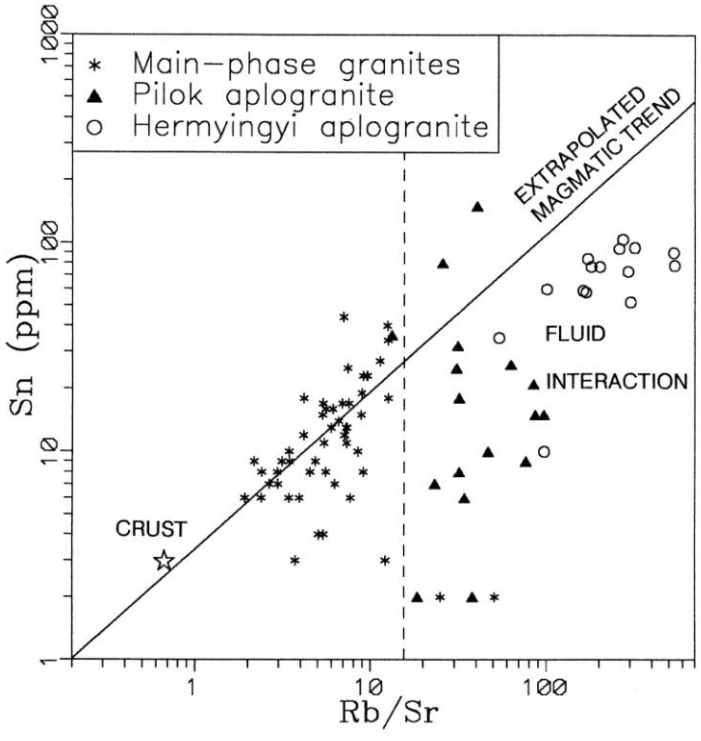
Main-phase granites
Pilok aplogranite
Hermyingyi aplogranite
EXTRAPOLATED
MAGMATIC TREND
FLUID
INTERACTION
CRUST
Sn (ppm)
Rb/Sr
1000
100
10
1
1
10
100

mining area, in which there is a volume of about 1 ± 0.5 km^3 of alkali-feldspar aplogranite. The tin potential of 1.5 ± 0.7 x 10^5 mt (tonnes) Sn, calculated on this theoretical basis, compares reasonably well with the cumulative production plus reserve figures for this area, which total approximately 5 x 10^4 mt Sn.

4.3 Ear Mountain, Alaska, USA

The 170-km-long, E-W-stretching tin belt on Seward Peninsula in Alaska is defined by nine posttectonic Late Cretaceous granite stocks which are associated with more or less tin mineralization of greisen, vein and skarn type and by placer tin accumulations (Hudson and Arth 1983). The largest primary tin deposit is Lost River with 33 Mio t of ore reserves at 0.29 % Sn (Taylor 1979). The metal potential of this tin province has been estimated at 550,000 t Sn (Reed et al. 1989).

The granites have high intrusion level and are mostly exposed in their uppermost roof portions only. The granite stock of the Lost River Mine has only subsurface outcrops, the Tin Creek pluton has a surface exposure of 0.2 km^2. The intrusions are composed of several texturally different biotite granite units with intrusive contacts. Their age is 70-80 Ma; Sr initials are in the range of 0.708-0.720 (Hudson and Arth, 1983). The granites have peraluminous composition (normative corundum 0.9-2.8 wt%); their composition plots at the low-pressure minimum of the experimental Qz-Ab-Or-H_2O system, and An contents are around 2-3 wt%. Chemical distribution patterns have systematics which suggest fractional crystallization as the dominant petrogenetic process during magmatic evolution, with fluid overprint in the most evolved granite phases (Hudson and Arth, 1983). REE patterns of the three major granite variants of the Seward Peninsula emphasize the importance of plagioclase fractionation (Eu/Eu* 0.15 already in the least-evolved granite unit), and of hydrothermal overprint (LREE and Eu depletion) (Fig. 58).

The 9-km^2-large Ear Mountain pluton is located in the middle part of the Seward tin belt and was studied in detail by Swanson et al. (1988). There are four biotite granite phases which define according to field relations and chemistry an intrusion suite of porphyritic → seriate → equigranular → fine-grained texture. The first two granite phases comprise 96 % of the pluton and consist of peraluminous biotite granite. The equigranular and fine-grained variants are biotite-muscovite granite with locally abundant tourmaline and

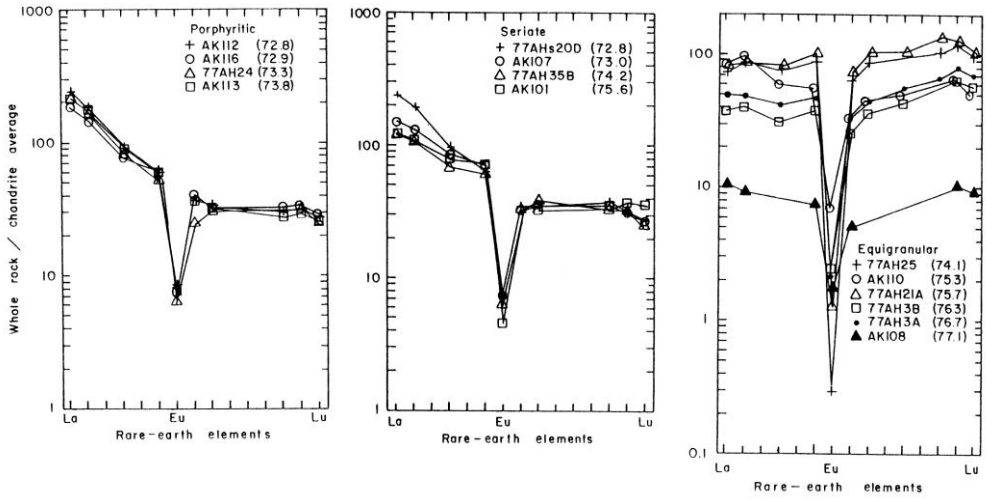

Fig. 58. REE patterns of the three major granite units of Seward Peninsula, Alaska. Intrusive sequence from porphyritic → seriate → equigranular texture. The symbols refer to individual granite samples (SiO_2 contents in brackets). (Hudson and Arth 1983)

fluorite, and occur in association with aplite/pegmatite veins and pods. Greisenization is locally and irregularly developed in all granite variants, and is characterized by a recrystallized mineral assemblage of quartz-muscovite-tourmaline with fluorite, cassiterite, rutile, pyrrhotite, pyrite, arsenopyrite and magnetite. Tin contents in greisen zones reach more than 1000 ppm and correlate positively with degree of fluid overprint.

Tin content of the four granite phases is shown in Fig. 59 as a function of TiO_2. The two least fractionated granite phases, though much more evolved than average low-Ca granite (Turekian and Wedepohl 1961), follow the general magmatic tin enrichment trend defined by Lehmann (1982). The most fractionated granite phases, on the other hand, are anomalously low in tin. They are modified by high-temperature fluid overprint (blastesis of muscovite, tourmaline, fluorite with feldspar stable), and their tin deficiency can be interpreted as a consequence of vapour exsolution/second boiling, a process which seems to be indicated by the fine-grained quench fabric of these rocks (Swanson et al. 1988). The inferred relationship of such high-temperature tin depletion with small-scale tin enrichment during feldspar-destructive greisenization at lower temperature or with fracture-controlled tin mineralization arises as a requirement of mass balance between the two interrelated systems "granite" and "tin mineralization".

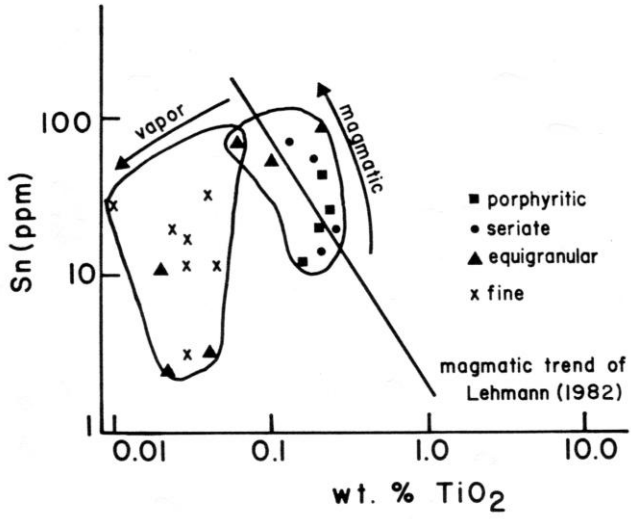

Fig. 59. TiO_2-Sn variation diagram for granite samples from the Ear Mountain Pluton, Seward Peninsula, Alaska. Magmatic tin enrichment trend and hydrothermal tin depletion by fluid interaction in the most fractionated granite phases. (Swanson et al. 1988:55)

4.4 Takua Pa, Southern Thailand

The Takua Pa pluton is part of the Phuket-Phangna mining district in southern Thailand which produces the major part of Thailand's tin. The average output of the Phuket-Phangna district over the last twenty years was 4000 t Sn/year, of which most tin is from placer mining. The primary deposits consist of low-grade disseminated greisens, quartz-cassiterite-wolframite veins, and Sn-Ta-bearing pegmatites. Petrography and geochemistry of the Takua Pa pluton was studied by Nakapadungrat et al. (1984a).

The Takua Pa pluton is a posttectonic and discordant, N-S-elongated intrusion (20 x 10 km) in a Permo-Carboniferous weakly metamorphosed and chiefly clastic sedimentary sequence. A four-point Rb-Sr isochron age is 78 ± 2 Ma with $^{87}Sr/^{86}Sr_i$ 0.7346 ± 6 (Nakapadungrat et al. 1984b), identical to the age of the Phuket granites (Putthapiban et al. 1986). The major part of the intrusion consists of several variants of K-feldspar megacrystic biotite granite with variable amounts of sub-solidus muscovite. Younger subintrusions consist of fine-grained biotite granite and of fine- to coarse-grained tourmaline-muscovite granite in which feldspar is partly replaced by muscovite and tourmaline (incipient greisenization).

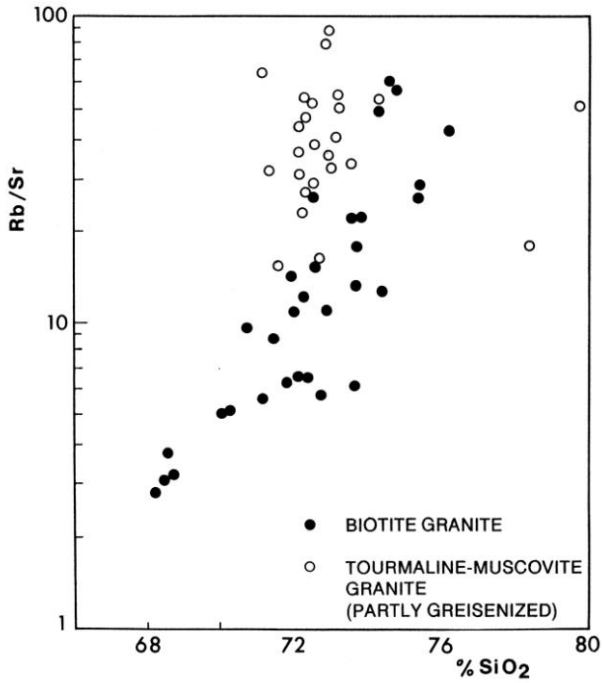

Fig. 60. SiO_2-Rb/Sr variation in samples from the Takua Pa pluton, southern Thailand. The biotite granite suite follows a magmatic differentiation trend, the tourmaline-muscovite granite suite has a fluid-modified scatter distribution. Data from Nakapadungrat et al. (1984a)

The normative composition of all rock units is peraluminous (biotite granite suite: 2 ± 1 wt% corundum) and lies close to the thermal minimum in the experimental Qz-Ab-Or-H_2O system at 0.5 kbar (An 5 wt%), which indicates advanced equilibration of melt composition with the high intrusion level. Systematic major and trace element distributions point to significant fractional crystallization of plagioclase and K-feldspar (Nakapadungrat et al. 1984a). The Rb/Sr-SiO_2 diagram of Fig. 60 gives a positive correlation trend for the biotite granite suite and a scatter distribution for the fluid-modified tourmaline-muscovite granite suite. The tin distribution in Fig. 61 is similarly composed of a systematic tin enrichment trend (dominantly magmatic) and a scatter distribution (fluid overprint) with tin contents up to subeconomic levels in most fractionated granite portions.

Fig. 61 (next page). Tin content as a function of TiO_2 and Rb/Sr in the Takua Pa pluton, southern Thailand. Systematic tin enrichment trend in the biotite granite suite with r[logSn-TiO_2] 0.58 and r[logSn-logRb/Sr] 0.69 (n=30), and scatter distribution in the fluid-modified tourmaline-muscovite granite suite. Data from Nakapadungrat et al. (1984a)

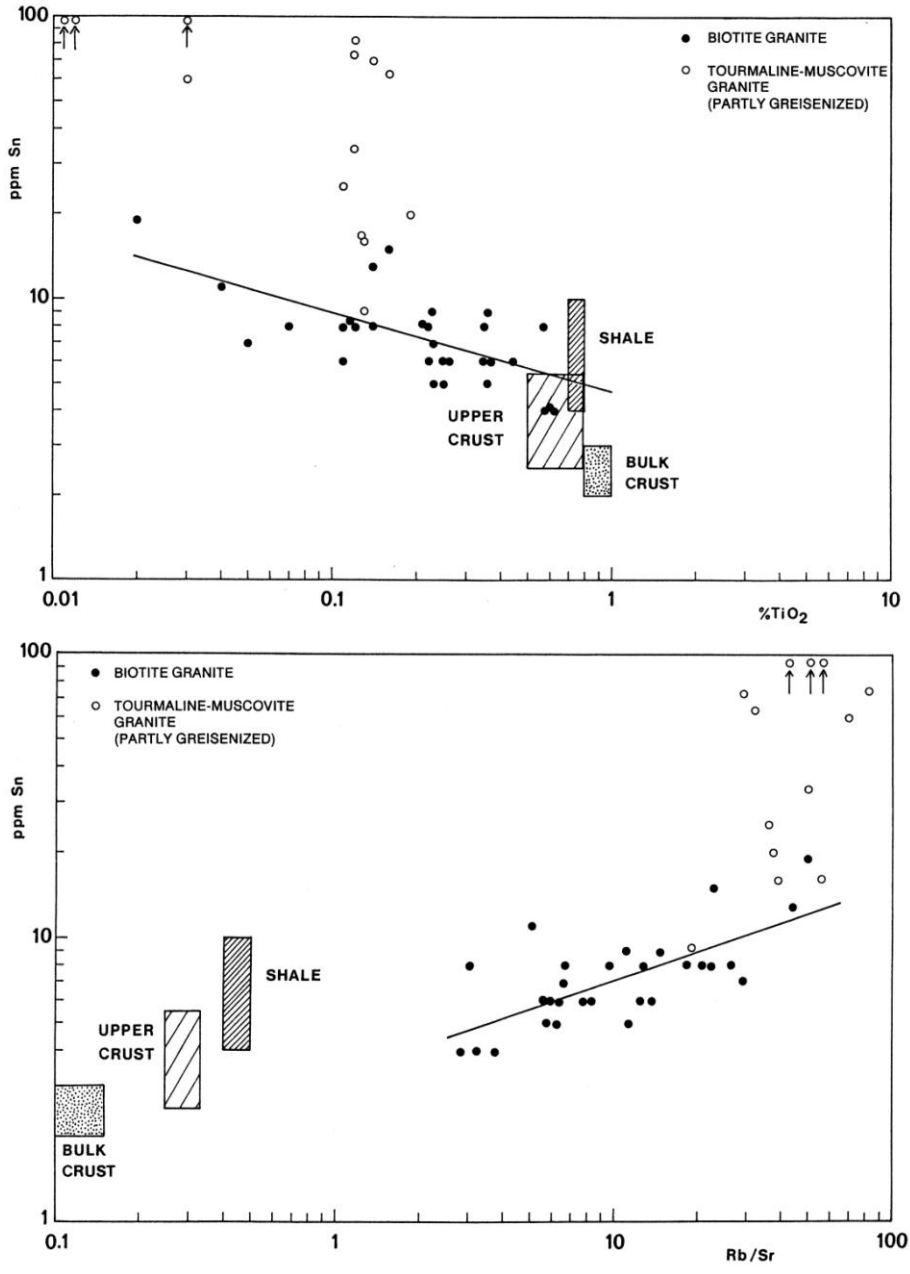

Fig. 61. For legend see previous page

4.5 Kinta Valley, Malaysia

The Kinta Valley with its mining centre of Ipoh is probably the largest tin field in the world and contributes around 30 % to the Malaysian tin production. Tin mining started only in 1876, but production since then has reached a cumulative figure near 2 Mio t Sn, which is about 10 % of the historic world tin output (Rajah 1979). Mining is essentially focussed on alluvial tin, with many small-scale gravel pump operations (up to 500 mines in prosperous times) and several dredges.

The Kinta tin field stretches over an area 90 km long and up to 25 km wide along the broad valley of the Kinta River and is surrounded in a horseshoe-shaped pattern by extensive granitic intrusions of the Main Range batholith of western Malaysia (Ingham and Bradford 1960) (Fig. 62). The local topography is controlled by the contrasting erosional resistivity of a limestone-dominated sedimentary sequence (Silurian to Permian) in the lower parts of the valley, and of Triassic granitic rocks in the surrounding mountain ranges with up to more than 1000 m of relief to the bottom of the valley. Primary tin mineralization of vein, stockwork, and greisen type is frequent; however, it is in general of a grade too low for hard-rock mining. Veinlets of the quartz-tourmaline-cassiterite mineral assemblage are ubiquitous in the granitic rocks.

The topographically striking Bujang Melakka pluton on the eastern edge of the Kinta Valley is an oval (20 x 10 km), N-S-trending granite intrusion with positive relief, surrounded by dozens of gravel pump mines which are mostly located at the deeply weathered granite-limestone contact. The major part of the pluton consists of K-feldspar megacrystic, medium-grained biotite granite with locally variable amounts of sub-solidus muscovite and tourmaline. Chiefly in the central part of the pluton, this granite phase is intruded by non-porphyritic muscovite granite of several textural varieties (Schwartz and Askury 1989). The Rb-Sr isochron age of the porphyritic main phase granite is 207 ± 14 Ma with $^{87}Sr/^{86}Sr_i$ 0.7193 ± 0.0024 (Darbyshire 1988a), fine-grained tourmaline granite has a K-Ar age on biotite of 203 ± 3 and 206 ± 5 Ma (Bignell and Snelling 1977). The Bujang Melakka pluton belongs to the ilmenite granite series (Ishihara et al. 1979; Fletcher et al. 1984) and samples least affected by hydrothermal overprint have a weakly metaluminous to weakly peraluminous composition (Schwartz and Askury 1989). Muscovite granite samples are - by definition - strongly peraluminous, and trace element patterns suggest both a high degree of fractionation and strong hydrothermal overprint.

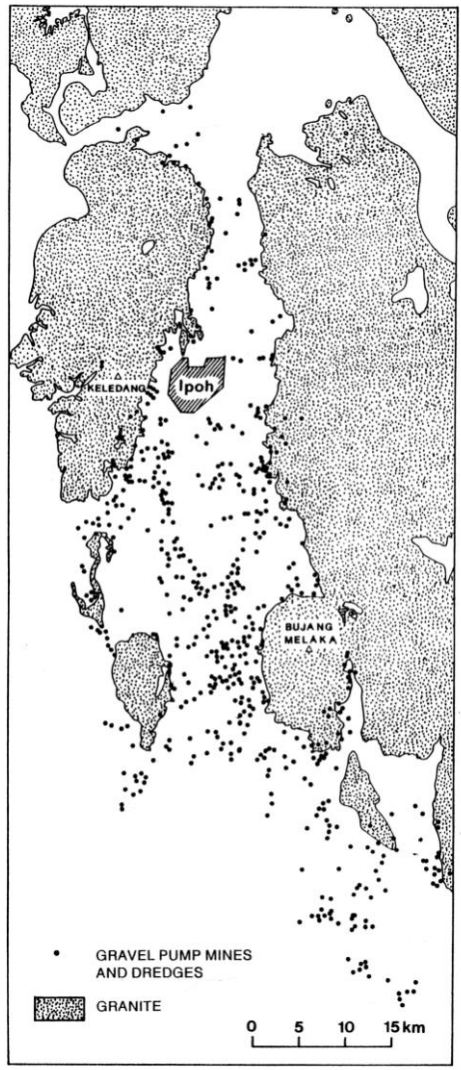

Fig. 62. Active tin mines in the Kinta Valley, Malaysia, during 1982-1985 (Geological Survey of Malaysia unpubl.). The tin deposits consist of alluvial placers and deeply weathered primary deposits, and are mined by hydraulic techniques, mostly small-scale gravel pump mining

The tin distribution pattern of the Bujang Melakka pluton and of some Main Range granites with less hydrothermal alteration is shown in Fig. 63. All granite samples have relatively high tin contents. The biotite granite samples, i.e. samples with low degree of hydrothermal alteration but ± sub-solidus muscovite as minor rock component, give a trend of linear correlation of log[TiO_2] versus log[Sn] with a large scatter, which suggests a pattern partly

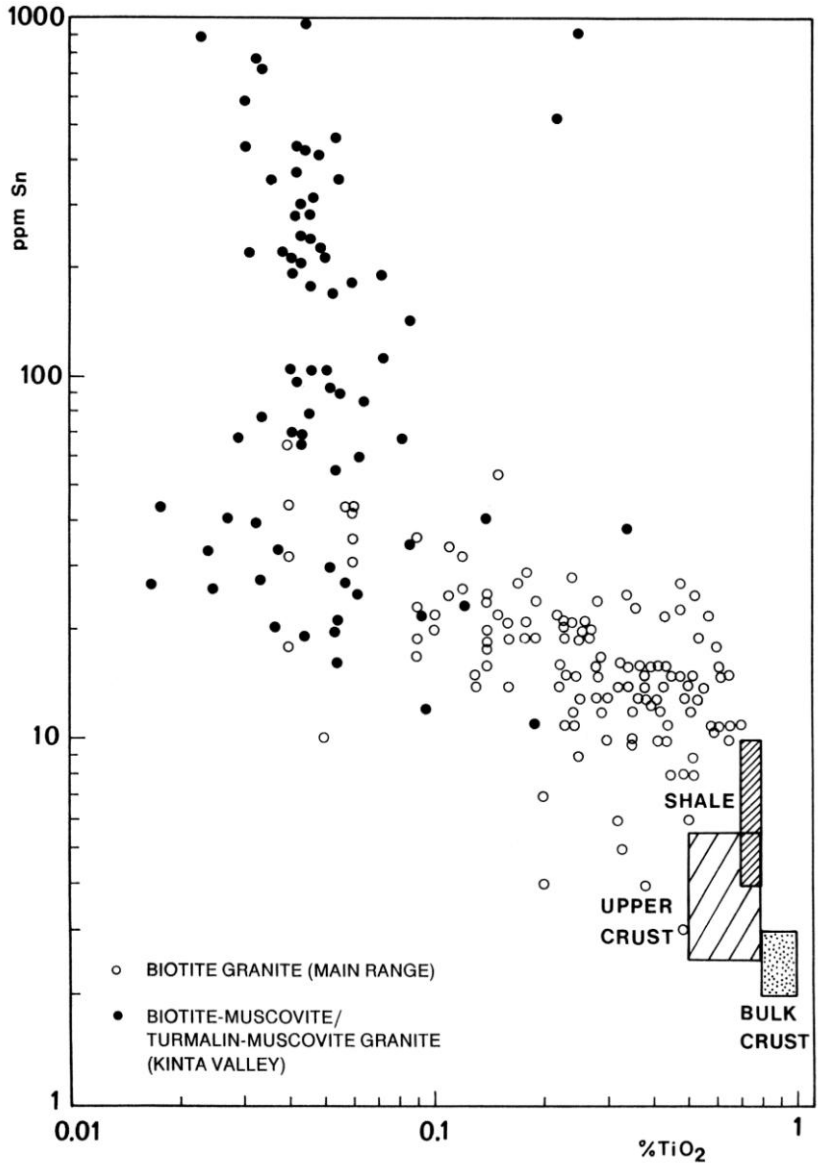

Fig. 63. Tin content as a function of TiO_2 (wt%) in granitic rocks of the Bujang Melaka pluton and other Main Range granites in Malaysia. Data from Liew (1983), Schwartz and Askury (1989), Cobbing (1989). Reference rock compositions from Rösler and Lange (1976), and Taylor and McLennan (1985)

controlled by magmatic fractionation and disturbed by secondary processes. A scatter-dominated pattern is developed in those samples which have tourmaline and/or muscovite as a major rock component. These rocks are

both highly fractionated (low contents of compatible elements) and are enriched in tin in an open system with presence of a fluid phase. Quartz-topaz greisen bodies reach subeconomic values of 0.3 % Sn and were formerly mined (Ulu Petai Mine; Ingham and Bradford 1960; Schwartz and Askury 1989).

4.6 Chacaltaya, Northern Bolivia

The Chacaltaya granite porphyry with around 0.5 km^2 in outcrop area is located 20 km north of La Paz. It forms the centre of a NW-SE-trending fossil hydrothermal system which is petrographically and geochemically traceable for 12 km in length and includes the mining areas of Milluni and Kellhuani (Lehmann 1985). Tin mineralization occurs in veins and in stratabound stockworks (mantos) which are lithologically controlled by the quartzitic members of a Silurian shale-metasandstone sequence. The Kellhuani mining area has proven plus indicated ore reserves of more than 9 Mio t with 0.5 % Sn (Lehmann 1979).

The Chacaltaya granite porphyry stock has a K-Ar age of 210 ± 6 Ma (McBride et al. 1983), contemporaneous with the Huayna Potosi batholith 8 km further north, and with other tin granites of the northern Bolivian tin belt. The Chacaltaya stock consists of porphyritic biotite granite with sub-solidus muscovite and is extensively affected by hydrothermal overprint. The most advanced product of the hydrothermal alteration spectrum is a heteroblastic, texturally homogenized quartz-muscovite rock without relics of primary-magmatic crystals preserved. These greisen bodies have irregular shape and are several tens of metres in size; tectonic control is not visible. Major rock components are quartz, muscovite, tourmaline, siderite, apatite, fluorite, sphalerite, pyrite, cassiterite and rutile.

The country rocks of the porphyry stock are hydrothermally transformed on a km scale, with a narrow halo of thermal metamorphism preserved relictically in some shale domains (muscovite-biotite-chlorite-quartz-andalusite). The hydrothermal aureole is in its inner part over a length of about 6 km characterized by the granoblastic mineral assemblage quartz-chlorite-tourmaline-fluorite-sericite/muscovite-siderite, the outer aureole differs from the regional-metamorphic reference system by more or less pronounced blastesis of quartz-chlorite-sericite-muscovite-siderite (Fig. 64).

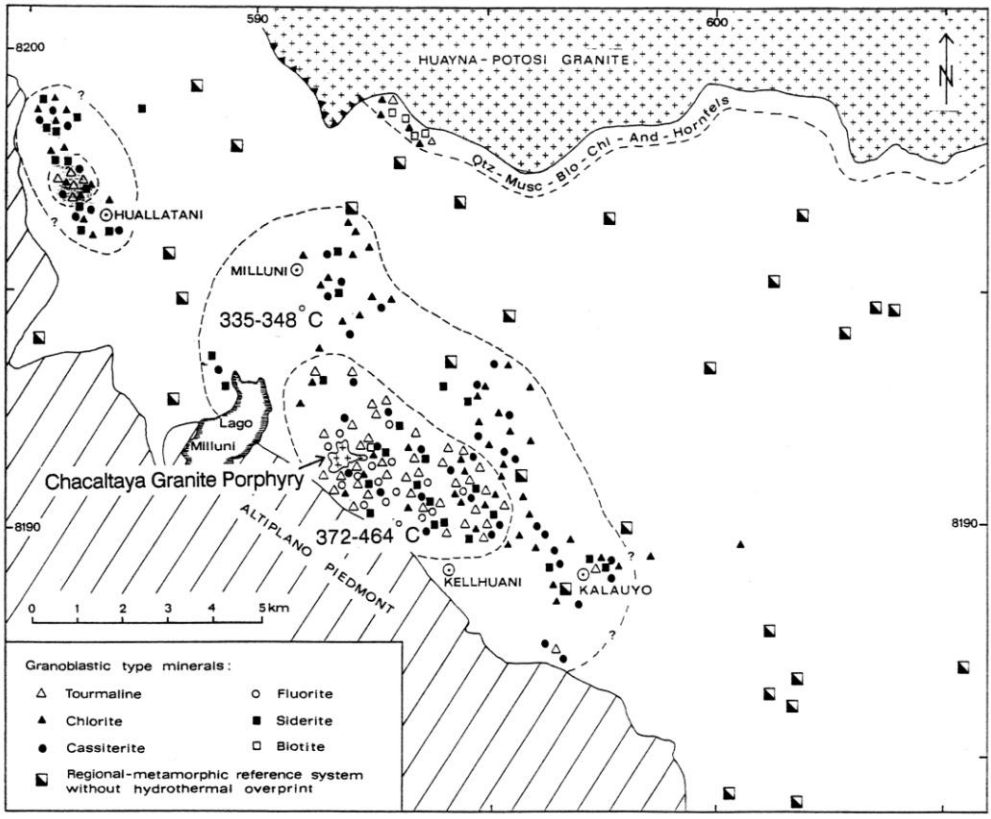

Fig. 64. The hydrothermal-alteration haloes in Silurian quartzites and shales around the Chacaltaya granite porphyry and in the area of Huallatani. The haloes define also the extent of the Kellhuani-Huallatani mining district. Cassiterite homogenization temperatures from Kelly and Turneaure (1970)

The dimensions of the hydrothermal halo are controlled by a fracture pattern of radial configuration which is centred on the porphyry stock and most developed near its contact zone where locally quartz-tourmaline and tourmaline breccias occur. The paleofracture pattern is accentuated by cm-large tourmalinization rims in the wall rocks, and is therefore easily distinguished from younger tectonic elements. The quartzitic fabric is a result of hydrothermal overprint and passes near the halo margin into a sandstone fabric with relatively little blastic grain modification. Stockworks are mostly confined to quartzitic strata, and the manto tin mineralization is located essentially on these closely spaced fractures (Fig. 65).

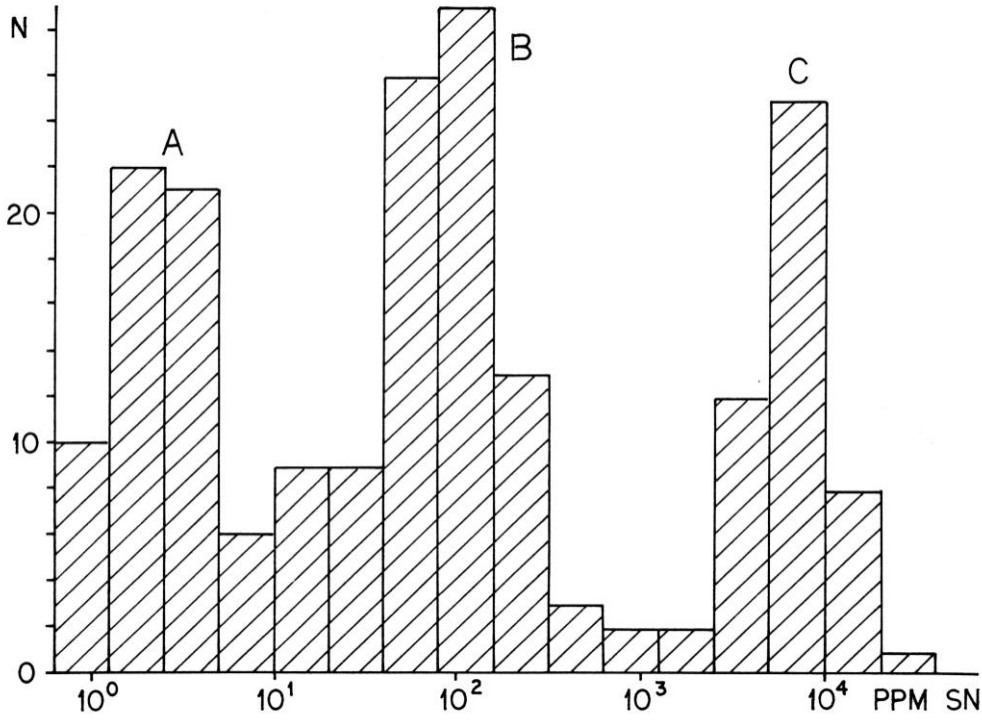

Fig. 65. Trimodal tin distribution in sedimentary rocks of the Kellhuani mining district. **A** regional background (3 ppm Sn); **B** hydrothermal overprint (100 ppm Sn); **C** stockwork/manto mineralization (0.3-1.0 wt% Sn). Data from Lehmann (1979), and Lehmann et al. (1988)

The typical mineral assemblage is quartz-tourmaline-cassiterite. Chlorite, fluorite, siderite, hematite, albite and muscovite are locally abundant. Sulfides are of minor importance; wolframite is restricted to the porphyry and its immediate vicinity. The temperature range of cassiterite crystallization in the Chacaltaya-Kellhuani area is 400-500°C, in the Milluni vein system temperatures of 380-430°C are recorded (Kelly and Turneaure 1970; salinity: 5-25 wt% NaCl equivalent; pressure: 0.5-1 kbar; see Lehmann 1985). The polymetallic sulfide mineral association (Zn-Cu-Bi-Pb) of the Milluni veins has a temperature of formation of <380 and >260°C. In the Kellhuani mantos, the polymetallic mineralization stage is developed on some larger fractures only. Permeability in the stockworks (fracture widths in the mm to cm range) seems

---

Fig. 66 (next page). Tin contents in granitic rocks from the Chacaltaya and Huayna Potosi intrusions as a function of TiO_2 and Rb/Sr. Data from Lehmann (1979)

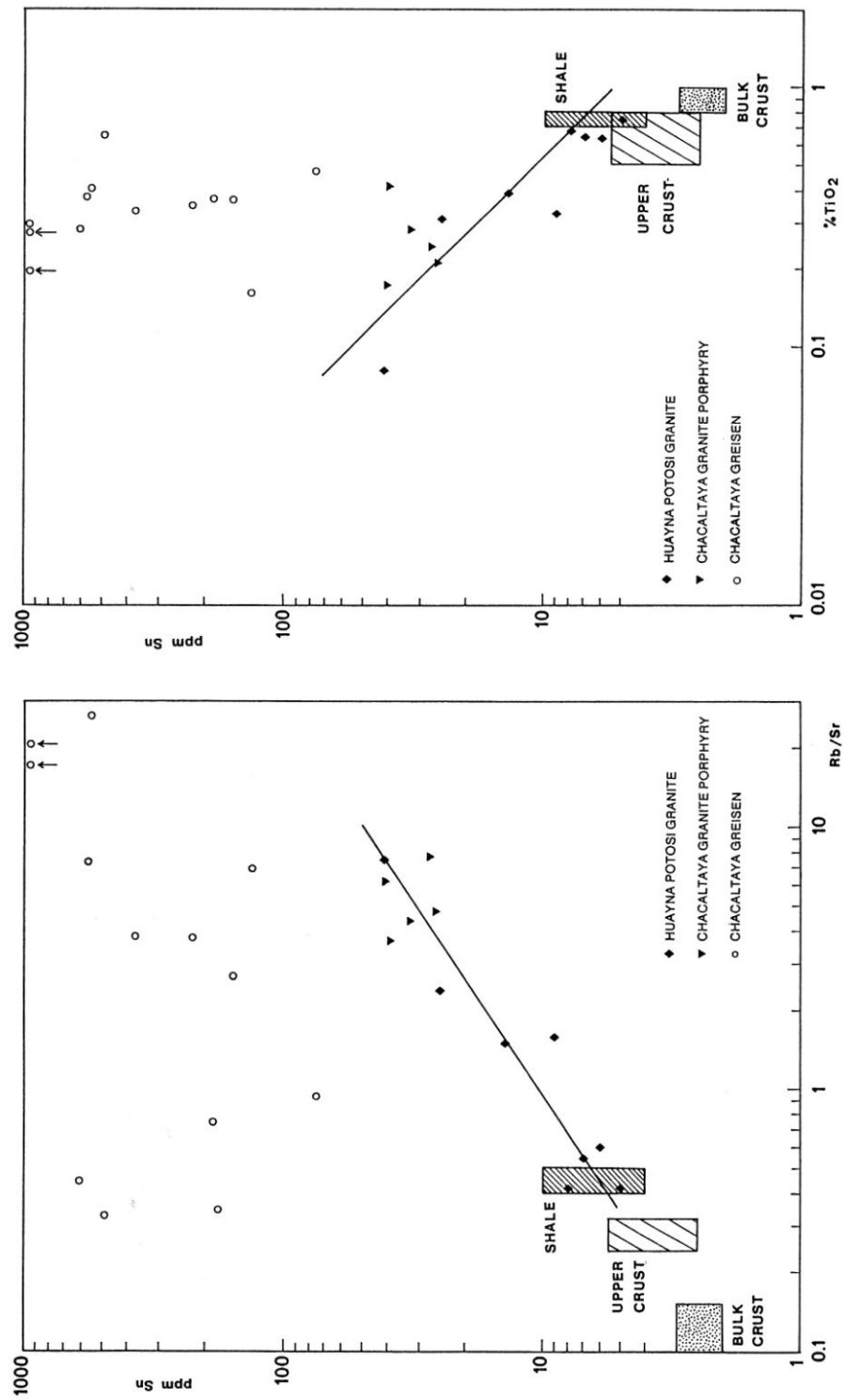
ppm Sn
1000
100
10
1
0.1
1
10
Rb/Sr
SHALE
UPPER CRUST
BULK CRUST
HUAYNA POTOSI GRANITE
CHACALTAYA GRANITE PORPHYRY
CHACALTAYA GREISEN
ppm Sn
1000
100
10
1
0.01
0.1
1
%TiO2
SHALE
UPPER CRUST
BULK CRUST
HUAYNA POTOSI GRANITE
CHACALTAYA GRANITE PORPHYRY
CHACALTAYA GREISEN

to have been reduced drastically already in the early stages of mineralization, whereas the longer-lived vein structures (dm to m range) allowed mineral deposition over a much larger time and temperature interval. The K-Ar age of hydrothermal muscovite of the manto tin mineralization is 213 ± 5 Ma and is identical to the age of the porphyry intrusion (McBride et al. 1983).

The large-scale halo pattern around the Chacaltaya porphyry can be defined both petrographically and geochemically. Primary dispersion haloes of Sn, F, B, Cs, Li or Zn have the same general configuration but variable, element-specific halo dimensions, with much larger dispersion patterns in the highly permeable quartzite units as compared to the shale units (Lehmann 1979).

There is still a magmatic tin pattern preserved in those samples of the Chacaltaya porphyry which have only moderate hydrothermal overprint. These samples, together with least-altered samples from neighbouring granitic intrusions define a primary tin enrichment trend (Fig. 66) which is

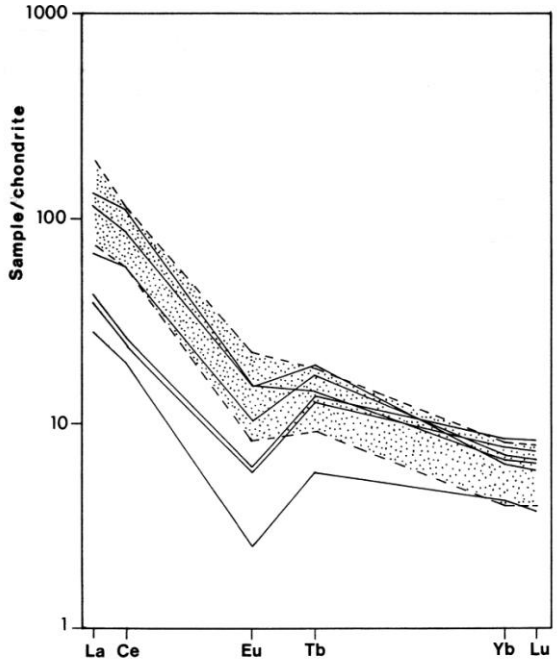

Fig. 67. REE distribution patterns for granitic samples from the Cordillera Real (solid lines) and ten greisen samples from the Chacaltaya granite porphyry (stippled field). Data from P. Dulski, Hahn-Meitner-Institut Berlin

identical to that of the larger Cordillera Real region of northern Bolivia discussed in Chapter 5.3. The strongly hydrothermally altered granite samples plot in a scatter field with generally elevated tin concentrations. Greisenization is not limited to highly fractionated granite portions but affects irregularly the whole range of granite compositions, which may indicate an external fluid source. The greisen samples have a REE distribution pattern identical to equivalent least-altered granite samples from the Cordillera Real (Fig. 67) which suggests very little REE mobility. Eu anomalies are not enhanced by fluid interaction in the Chacaltaya greisens, contrary to the behaviour of Eu during sericitic alteration in the Cornwall tin province (Alderton et al. 1980).

4.7 Chorolque, Southern Bolivia

The Chorolque tin porphyry deposit is located in the southernmost part of the Bolivian tin belt, and has been a tin producer since 1870. Minor amounts of tungsten, bismuth, lead and zinc have been produced from small peripheral veins. Subeconomic silver and gold values are known but are not recovered (Ahlfeld and Schneider-Scherbina 1964). Chorolque is one of the numerous subvolcanic polymetallic mineralization centres in southern Bolivia (Cerro Rico de Potosi, Tasna, Chocaya, Tatasi etc.) which are all of Upper Miocene age with 12-17 Ma, and are thus different from the Early Miocene (>20 Ma) tin porphyry systems further north (Llallagua, Colquechaca, Morococala etc.) which are eroded more deeply (Grant et al. 1979).

The Chorolque igneous complex consists of a largely brecciated circular volcanic vent about 1 km in diameter, which is surrounded by rhyodacitic lavas and tuffs, and which cuts through a peneplain of Ordovician shale basement with a presentday elevation of 4000 m. The vent area is intensively overprinted by quartz-tourmaline alteration, and forms an erosionally resistant peak with the summit at 5600 m. The heteroblastic quartz-tourmaline alteration zone in the central part is surrounded by a sericite-pyrite alteration halo which extends up to 600 m from the intrusive contact into the volcanic and sedimentary rocks and passes gradually into an outer shell of propylitic alteration (biotite → chlorite) (Fig. 68). Tin mineralization is essentially on quartz-tourmaline-cassiterite veins and veinlets confined to the central part of the hydrothermal system. Low-grade disseminated tin mineralization with a polymetallic mineral association of pyrite-arsenopyrite-chalcopyrite-bismuthinite-stannite-cassiterite is located mostly in the peripheral sericite-

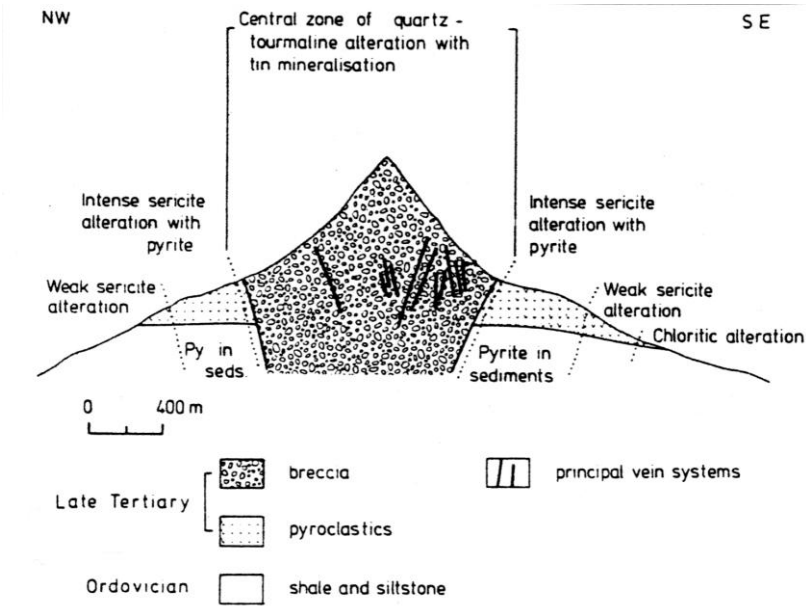

Fig. 68. Schematic cross-section of the Chorolque tin porphyry and its hydrothermal alteration pattern. (Grant et al. 1977:120)

pyrite alteration zone. The geochemical dispersion patterns of Sn, Ag, Bi and Cu are given in the cross-sections of Fig. 69.

Fluid inclusion studies by Grant et al. (1977) demonstrate that the quartz-tourmaline alteration in the core zone of the hydrothermal system developed at a minimum temperature of 500°C and was accompanied by boiling of a saline fluid (co-existence of vapour and liquid phases with >60 wt% NaCl). Cassiterite crystallization is related to lower temperature of 300-250°C and lower salinity (<26 wt% NaCl), and is synchroneous with pervasive sericitization. Stable isotope data suggest that this stage of tin mineralization and sericitic alteration was dominated by meteoric water whereas the early high-temperature and high-salinity tourmalinization was dominated by a magmatic fluid phase (Grant et al. 1980).

The temperature-salinity evolution of the tin porphyry system of Chorolque and the much larger Llallagua system are compiled in Fig. 70. Grant et al. (1977, 1980) propose a general genetic model which is very near the model of Burnham (1979a) for copper porphyry deposits: explosive release of an aqueous, Cl- and B-rich fluid phase during the high-level crystallization of a dacitic to rhyolitic melt which leads to pervasive brecciation (hydraulic fracturing) and high-temperature tourmalinization; metal deposition as a consequence of mixing of the magmatic fluid phase with a cooler meteoric

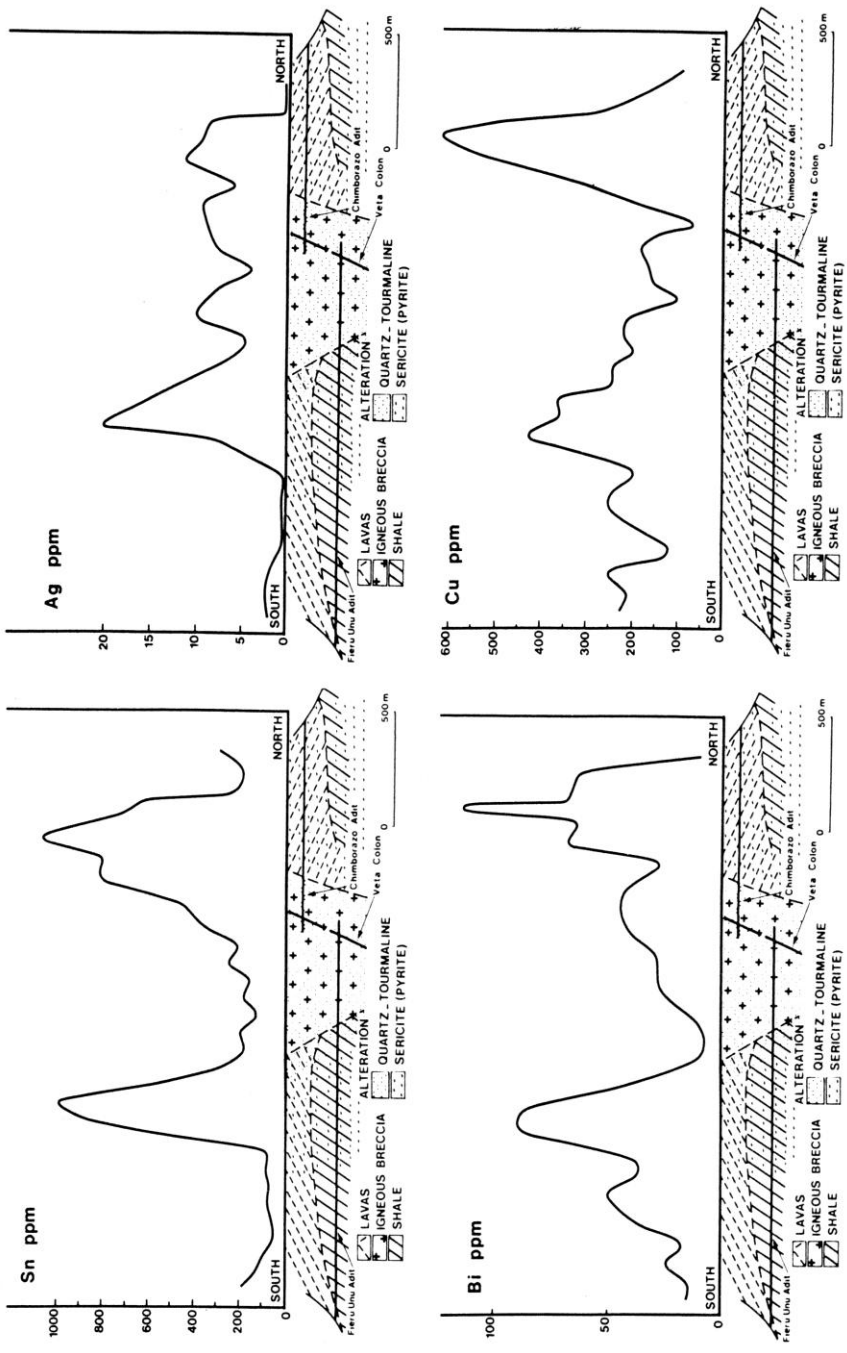

Fig. 69. Geochemical cross-sections through the Chorolque tin porphyry. (Grant et al. 1977:121)

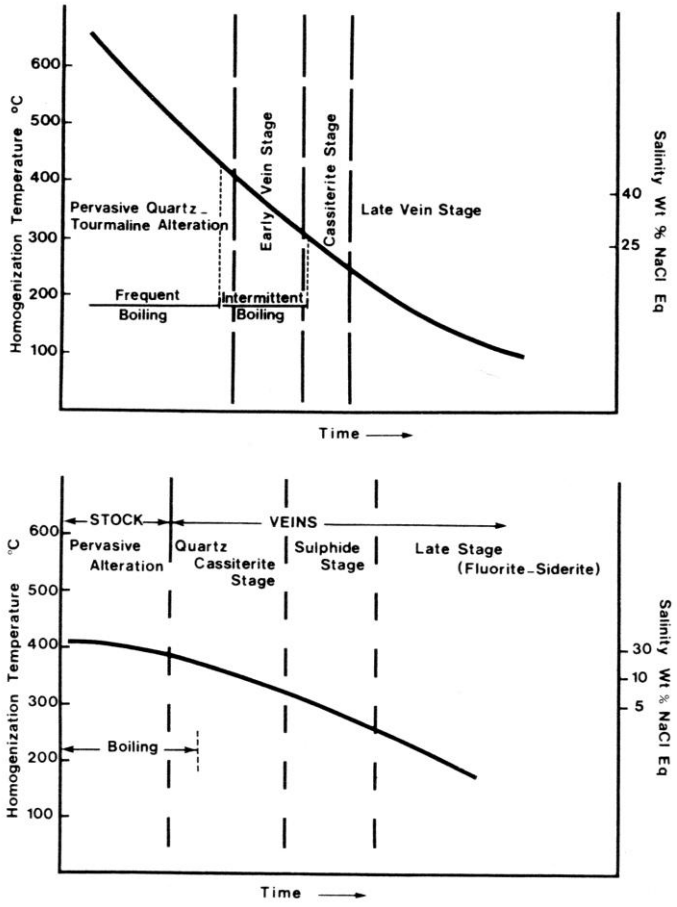

Fig. 70. The temperature-salinity evolution of the hydrothermal systems of the Chorolque (upper diagram) and Llallagua (lower diagram) tin porphyries, reconstructed from fluid inclusion data. (Grant et al. 1977:124)

fluid of low salinity. Recurrent intrusive activity may lead to repetitive patterns of mineralization, with the locus of release of magmatic fluids from a fractionating and crystallizing large-scale magma chamber progressively shifting towards deeper crustal levels.

The magmatic history of the tin porphyries is relatively little known due to pervasive hydrothermal transformations which in many cases do not even permit a reliable petrographic classification of the pre-hydrothermal magmatic material. The magmatic evolution of tin is correspondingly obliterated. This problem will be addressed in Chapter 5.3 on the regional tin distribution pattern of the Bolivian tin province.

Tin porphyries are not limited to Bolivia but are known from the Sierra Madre Occidental in central Mexico, southern China and eastern Siberia as well (Ypma and Simons 1969; Pan 1974; Ruiz 1988; Magak'yan 1968; Guan Xunfan et al. 1984; Yang Shiyi et al. 1984). Subeconomic tin concentrations occur in fluorine-rich, high-silica rhyolites widely distributed over the western USA, known as topaz rhyolites (Burt et al. 1982). The extreme degree of fractionation of the tin-bearing rhyolites of the Mexican tin belt and of the topaz rhyolites in the USA has been documented by Huspeni et al. (1984), Ruiz (1988), and Christiansen et al. (1983). The in general low-grade tin concentrations (≤0.1 wt% Sn) are associated with subvolcanic breccia and stockwork zones in Oligocene rhyolite flows and domes. The locally fayalite-bearing rhyolites (→low *f*O2) are metaluminous to slightly peraluminous, have initial Sr isotope ratios of 0.705-0.708, and are enriched in a suite of incompatible trace elements such as Sn, F, B, U, Th, Rb, Zn, Cs, As (Pan 1974; Burt et al. 1982; Huspeni et al. 1984). The REE spectra in Fig. 71 indicate an advanced degree of plagioclase fractionation.

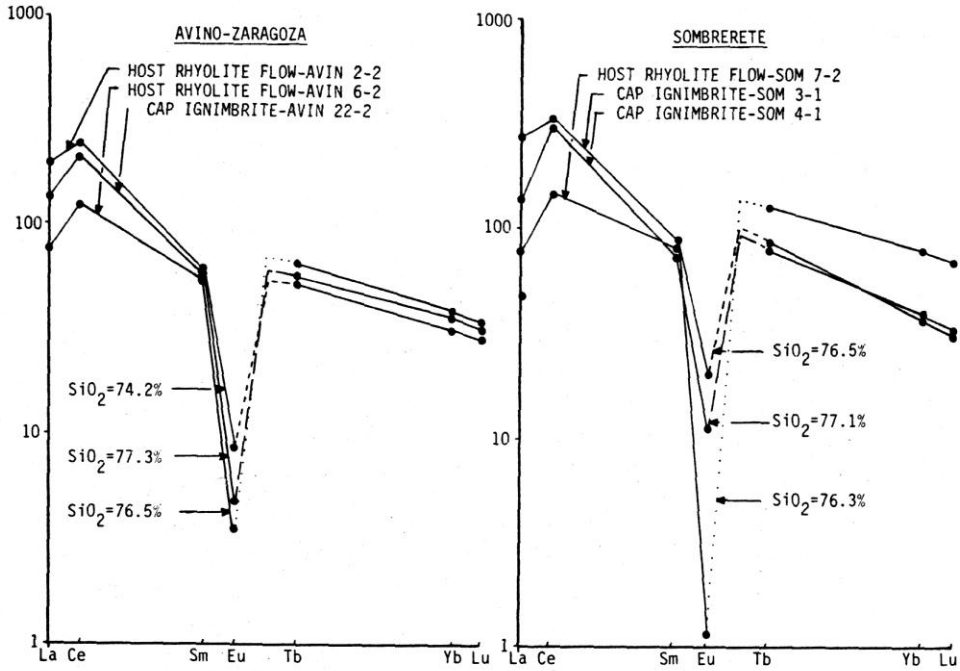

Fig. 71. REE distribution patterns of tin-bearing rhyolites of the Durango tin-ilver mining district in Mexico. (Huspeni et al. 1984:102)